

We are IntechOpen, the world's leading publisher of Open Access books Built by scientists, for scientists

4,800

Open access books available

122,000

International authors and editors

135M

Downloads

Our authors are among the

154

Countries delivered to

TOP 1%

most cited scientists

12.2%

Contributors from top 500 universities



WEB OF SCIENCE™

Selection of our books indexed in the Book Citation Index
in Web of Science™ Core Collection (BKCI)

Interested in publishing with us?
Contact book.department@intechopen.com

Numbers displayed above are based on latest data collected.
For more information visit www.intechopen.com



The Genesis of the Mississippi Valley-Type Fluorite Ore at Jebel Stah (Zaghouan District, North-Eastern Tunisia) Constrained by Thermal and Chemical Properties of Fluids and REE and Sr Isotope Geochemistry

Fouad Souissi^{1,2}, Radhia Souissi² and Jean-Louis Dandurand³

¹*Département of Geology, Faculty of Sciences, University El Manar*

²*Institut National d'Analyses Physico-chimiques (INRAP), Sidi Thabet*

³*University of Toulouse, UPS (OMP), LMTG, Toulouse*

^{1,2}*Tunisia*

³*France*

1. Introduction

The fluorite district of Zaghouan, North-eastern Tunisia (Fig. 1), is characterized by occurrences of F-(Ba-Pb-Zn) mineralization associated with uplifted blocks of Jurassic reef limestone. The host rocks belong to the Hettangian-Lower Sinemurian Oust Formation and the Kimmeridgian-Tithonian-Berriasian Ressas Formation, capped by emergence surfaces and layers of condensed phosphate-bearing rocks. The uplifted blocks belong to the Jurassic mountain area; most of which run along the Zaghouan Fault (Turki, 1988), which extends over 80 km along the NE-SW Atlas fold trend with a vertical throw of 4,000 to 5,000 m. The Zaghouan Fault is considered to be a major lineament of the African block (Richert, 1971), behaving as a reverse fault crosscutting both the basement and the sedimentary cover (Castany, 1954). Local brecciated and chaotic masses of evaporates, claystones and black dolostones of Triassic age outcrop along the fault. No post-Triassic magmatic or metamorphic events have been reported in the region.

The F-(Ba,Pb,Zn) deposits of the Zaghouan district (Fig. 1) consist of stratabound and/or stratiform bodies, either within or immediately above, the Jurassic reef limestones, along unconformity surfaces (shoals, condensed layers, stratigraphic gaps, karst or paleosol features) which separate the Oust Formation (Stah, Kohol), or the Ressas Formation (Zriba-Guebli, Mecella), from the overlying series. Mineralization may also occur within fractures crosscutting the limestone uplifted blocks and their overburden (Hammam Jedidi, Oust, Sidi Taya). Despite the gross similarity of the Liassic series throughout the major part of the district (Stah, Kohol, Oust, Zaress, Bent Saidane, Fkirine; Fig. 1), stratabound fluorite deposits featuring a strong epigenetic dolomitization of the country rocks, are known only from the locality of Jebel Stah and in the neighbouring area of Jebel Kohol.

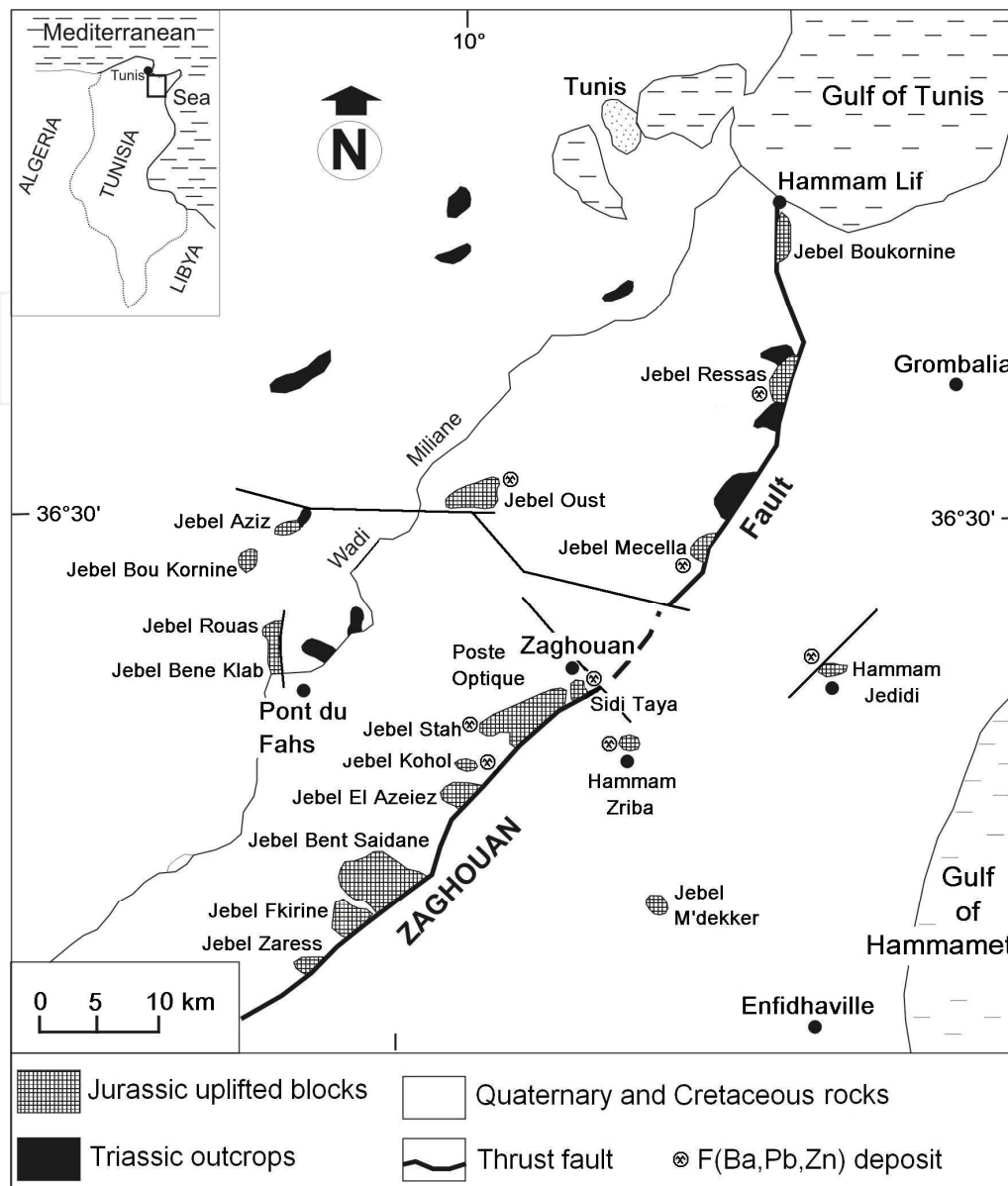


Fig. 1. Location map showing the Jurassic uplifted blocks and Triassic outcrops, along with F-(Ba,Pb,Zn) deposits, in North-eastern Tunisia.

Using detailed petrographic description of the fluorite ore bearing rocks, fluid inclusion (FI) microthermometry, metallic trace element (MTE), rare earth element (REE) and Sr isotope geochemistry, the authors reconstruct the geological history of the mineralization and propose a genetic model for the fluorite deposit of Jebel Stah.

2. Geological setting

Field observations show that the lithostratigraphic successions associated with ore-bearing series and barren equivalents are significantly different. The lithostratigraphic column at Jebel Stah (Figs. 2 and 3) consists of the complete stratigraphic sequence between the Lower Liassic and the Lower Cretaceous. Mineralization occurs both in the upper part of the Oust Formation (grey Hettangian-Lower Sinemurian limestones) which forms an uplifted block,

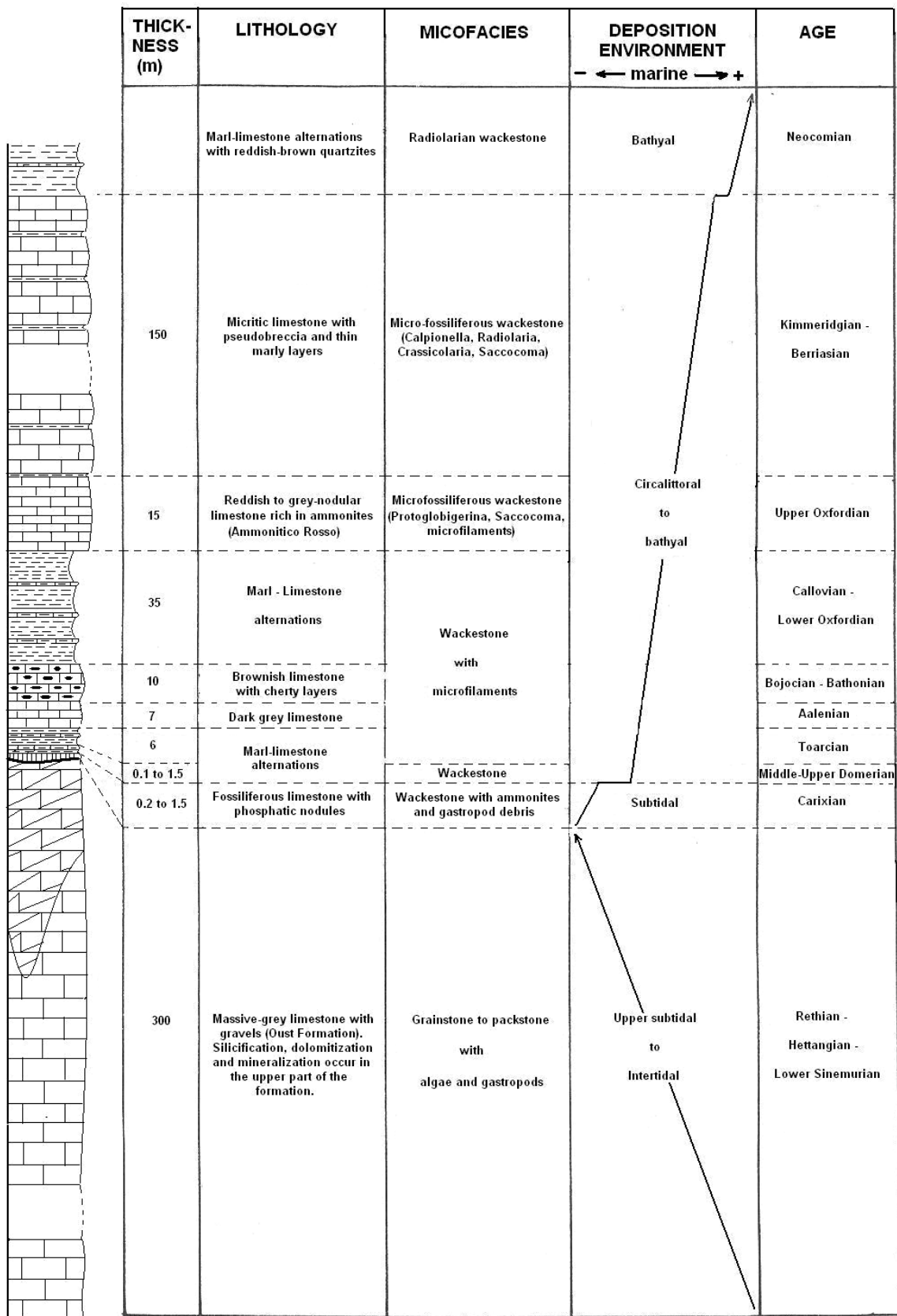


Fig. 2. Lithostratigraphic column of Jebel Stah and its petrographic, paleoenvironmental and chronological characteristics.

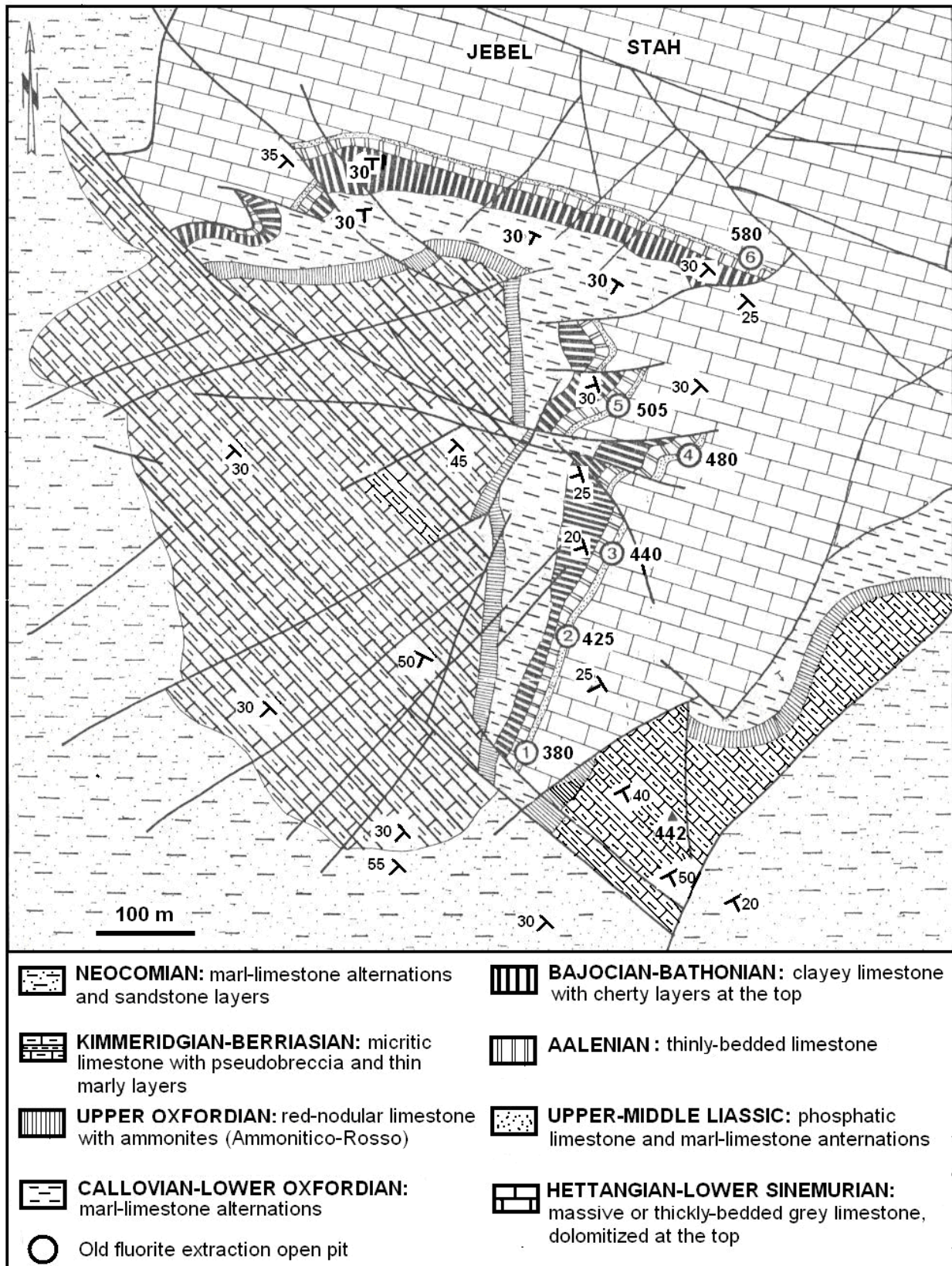


Fig. 3. Geological map of Jebel Stah (modified after the Office National des Mines "ONM", 1968).

as well as within the overlying Carixian layer. The upper part of the Oust Formation limestones underwent diagenetic silicification and a subsequent strong dolomitization. The Oust Formation is overlain by an emergence surface evidenced by a hard ground and small karstic cavities. The Middle-Upper Carixian condensed layer (0.2 to 1.2 m thick) overlies the Oust Formation and consists of lenticular limestones rich in phosphatic nodules, ammonites and gastropods, and in grains of glauconite and authigenic quartz. The limestone beds are covered by a pyritic crust a few mm in thickness. Detrital silico-carbonate deposits, accumulated in karstic cavities at the top of the Oust Formation, provide evidence for a second emergence phase during the Lower Dimerian period (Rakus and Biely, 1970). The overlying Middle-Upper Dimerian to Neocomian series is represented by an alternation of marls and limestones.

At Jebel Stah and Jebel Kohol, ore mainly consists of fluorite and calcite. Other minerals are also present (sphalerite, galena, barite, celestite, malachite, azurite, siderite, ankerite, quartz), albeit sporadically.

At Jebel Stah, fluorite used to be extracted in open pits (Fig. 3), from 1937 to 1942 (6,500 tons; Sainfeld, 1952). The same pattern emerged again from 1969 to 1974 (60,000 tons; ONM, 1990), to provide ore grading 70% CaF₂ that could be marketed for metallurgical use. It is, however, interesting to note that exploration programs, conducted by ONM (1990), have shown that the adjacent Jebel Kohol deposit contains in excess of 230,000 tons of certified ore reserves and 76,000 tons of probable reserves, grading 29% CaF₂, 2% Pb and 2% Zn.

At Jebel Oust (Figs. 1 and 4), like at Jebel Stah, the Oust limestones are overlain by the Carixian condensed phosphatic limestone unit showing a ferruginous crust and a slight karstification at the top. Authigenic quartz is scarce and no dolomitization occurs in the upper part of the Oust Formation. The Carixian layer is overlain by the Upper Jurassic (Callovian to Tithonian) marl-limestone sequence. Mineralization mainly consists of fluorite with accessory Cu-bearing sulphosalts occurring within a vertical to sub-vertical extensive fault system induced by a NW-SE strain (σ_1) and related to the Late-Miocene compressive phase. The N160°-180°E direction fits with the extensive faults s.s., while those trending N010°-030°E and N090-110°E behave as sinistral and dextral strike-slip faults, respectively. The fractures cut through the Lower-Middle Liassic, the overlying Upper Jurassic series, and extend to the Lower Cretaceous units (Souissi et al., 1996).

In contrast to the above, the Lower-Middle Liassic units at the Poste Optique (at the ENE limit of Zaghouan Mountain, almost 5 km from Jebel Stah; Fig. 1) consist of a thick, complete and non-fossiliferous sequence (Fig. 4). Ore occurrences are totally absent in this area (Souissi, 1987).

3. Host rocks and ore petrography

The mineralization of Jebel Stah runs along the Middle-Liassic unconformity. Several distinct types of orebodies are recognized (Fig. 5): (i) stratabound ores constitute the economic volume of the deposit and run along the unconformity surface, occurring as replacement clusters or open space fillings in the Carixian layer, but also in the upper part of the Lower Liassic and at the bottom of the Middle-Upper Dimerian rocks in the hanging wall as small lenses (20 to 40 cm long and a few mm thick) replacing thin carbonate layers; (ii) fracture-controlled mineralization within vertical extensional veins which cut the entire

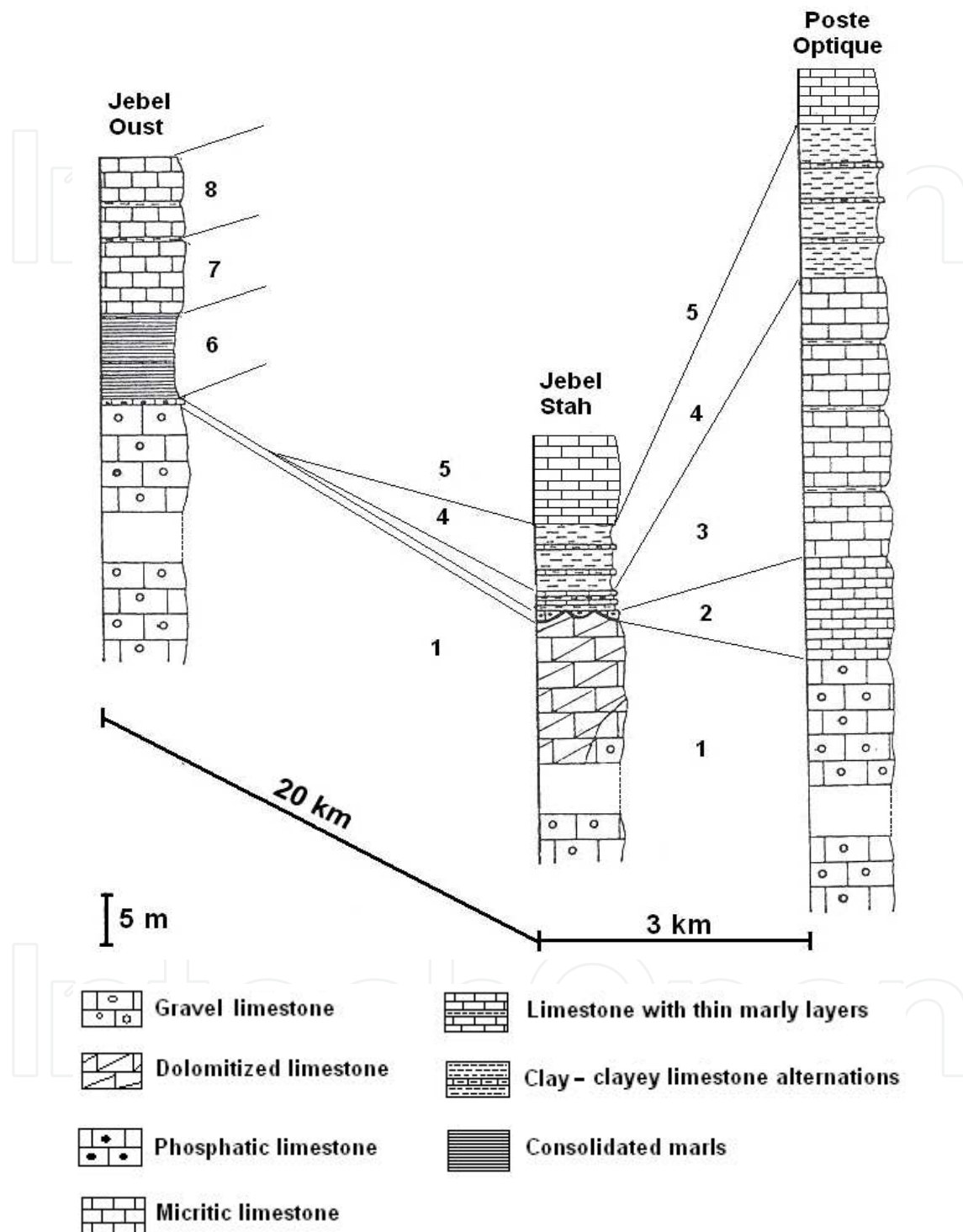
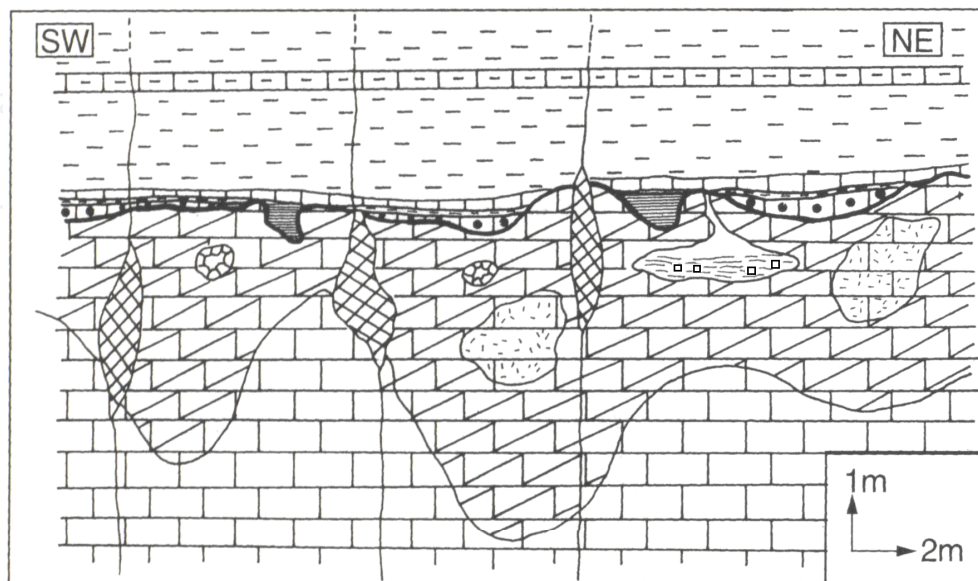


Fig. 4. Correlation between the Liassic series of Jebel Stah and Poste Optique (Zaghouan) and Jebel Oust (1: Hettangian-Lower Sinemurian, 2: Carixian (Upper Sinemurian-Carixian at Poste Optique), 3: Domerian (Middle-Upper at Jebel Stah), 4: Toarcian, 5: Aalenian, 6: Callovian-Lower Oxfordian, 7: Upper Oxfordian, 9: Kimmeridgian-Lower Tithonian).







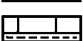
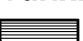
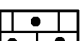

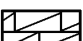
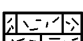
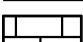
-  Fluorite in geode (FI3)
-  Intradolomitic solution void with pelites and cubic fluorite (FI3)
-  Breccia fillings with calcite and fluorite within vertical lodes (FI2)
-  **Toarcian:** Clays and marly limestones
-  **Domerian:** clays and marly limestones (dolomitized and mineralized in their lower part)
- Carixian**
-  Karstic cavities with dolomitized sediments replaced by fluorite (FI1a, b)
-  Phosphatic limestones (partially dolomitized and mineralized) (FI1a, b)
- Hettangian-Lower Sinemurian**
-  Hard ground
-  Reddish dolostone (mineralized in its upper part (FI1a, b)
-  Grey limestone with authigenic quartz
-  Grey limestone

Fig. 5. Schematic cross-section of the Lower-Middle Liassic sequence at Jebel Stah showing the location and the morphology of the fluorite orebodies. FI1a, FI1b, FI2 and FI3 are petrographic types of fluorite (after Souissi et al., 1997, 1998).

Liassic series, where large openings are created and filled with fluorite and sparry calcite; (iii) fluorite within cavities; and (iv) accessory fluorite and massive smoky quartz within fractures.

The country limestones of the Oust Formation are characterized by grainstone to packstone microfacies rich in green and incrusting algal debris (*Paleodasycladus* and *Thaumatoporella*, respectively), oncolites and skeletons of foraminifera (Fig. 6A, B). This facies indicates sedimentation under strong hydrodynamic conditions. The abundance of the green algae indicates a shallow water environment, probably in a back reef zone. Near the top of the formation, the presence of fibrous calcite, surrounding the framework grains, indicates a deposition in a vadose environment; while the abundance of dissolved gypsum crystals molds and authigenic quartz crystals (Fig. 6C) provide evidence that pre-evaporitic conditions prevailed. The product of dolomitization consists of a reddish, homogeneous dolosparite extending beyond the emergence surface, and partially affecting the Carixian and Domerian units. The crystallization of dolomite after quartz (Fig. 7A) and the emergence phases (Fig. 8A) testify to its late diagenetic to epigenetic origin. The top of the dolomitic horizon consists of an anisotropic facies occurring as banded (Fig. 7B) or solution-breccia (Fig. 7C) structures, and consisting of a dark-coloured dolosparite, similar to the one described above, and associated with a light-coloured (yellow to white) dolomacrosparite of antipolar growth.

All dolomite types show a sweeping extinction between crossed polars. This petrographic type of dolomite is known as “ferroan dolomite” (Choquette, 1971); “baroque dolomite” (Folk and Assereto, 1974); “sparry dolomite” (Beales and Hardy, 1980), “saddle dolomite” (Radke and Mathis, 1980), or “xenotopic dolomite” (Gregg and Sibley, 1984). Radke and Mathis (1980) and Gregg and Sibley (1984) considered that this type of dolomite crystallizes after burial, at temperatures ranging from 50-60 °C to 100-150 °C. According to Beales (1971) and Choquette (1971) these dolomites crystallize in the same conditions as the associated ore minerals.

The banded dolomites are known in the literature as “franciscaine” (Jacquin, 1970; Trona, 1973), “banded spar” (Martini, 1976), “Zebra texture” (Beales and Hardy, 1980), “diagenetic crystallization rhythmites or DCRS” (Fontboté, 1981; Fontboté and Amstutz, 1983), “Zebra rock” (Spangenberg et al., 1993; Spangenberg et al., 1995). This petrographic type of dolomite is similar to those present within the gangue of several Pb-Zn-Ba-F Mississippi Valley type (MVT) deposits, where they always accompany the ore minerals (Beales and Hardy, 1980; Ohle, 1985; Fontboté and Gorawski, 1990; Fontboté, 1993). According to Fontboté and Gorawski (1990) the DCRs result from the interaction of hot brines within the host rocks in an open system, long after the lithification; these brines are similar to those giving rise to the Mississippi Valley ore deposits.

The mineralization consists mainly of four distinct petrographic types (Table 1). Ore types Fl1a and Fl1b occur within the stratabound ore bodies, type Fl2 corresponds to the fluorite in the sub-vertical lodes (Fig. 5) and type Fl3 corresponds to fluorite occurring in cavities.

Fl1a. Replacement clusters which may be considered as the early fluorite generation. They are closely connected in space to the epigenetic dolomitization of the host rocks (Souissi et al., 1998). This facies consists of a microgranular (sub-mm- to mm-sized) fluorite and occurs

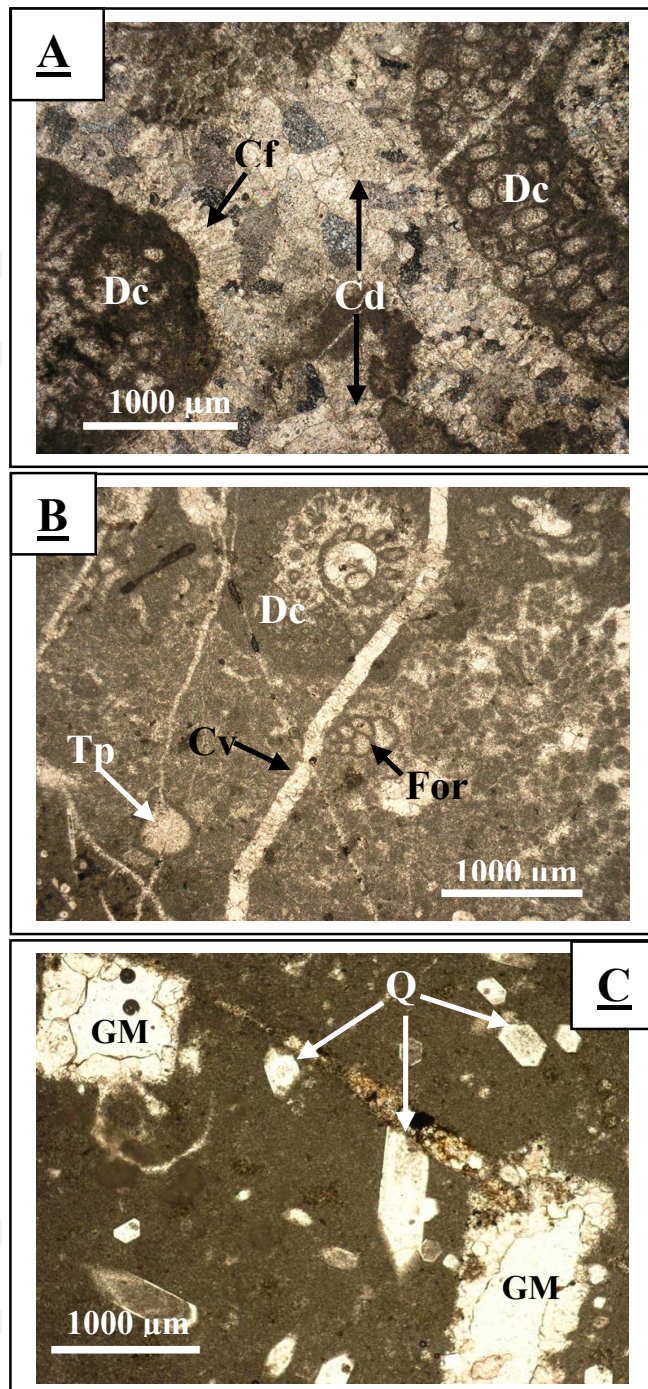


Fig. 6. Petrography of the grey limestone country rocks of the Hettangian-Lower Sinemurian, in thin sections. (A) Grainstone rich in green algal (Dasycladals: Dc) debris (sample L5-8, crossed polars). Note that the grains are surrounded by fibrous calcite (Cf). Voids are cemented by a drusy calcite (Cd). (B) Grainstone to packstone including green algal (Dasycladals "Dc") and red algal (Thaumatoporels "Tp") debris and foraminifera tests (For), crosscut by a calcite vein (Cv), (sample JSII-14; polarized light). (C) Carbonate matrix (M) including authigenic quartz (Q) and gypsum molds (GM) (sample JS3-8, polarized light).

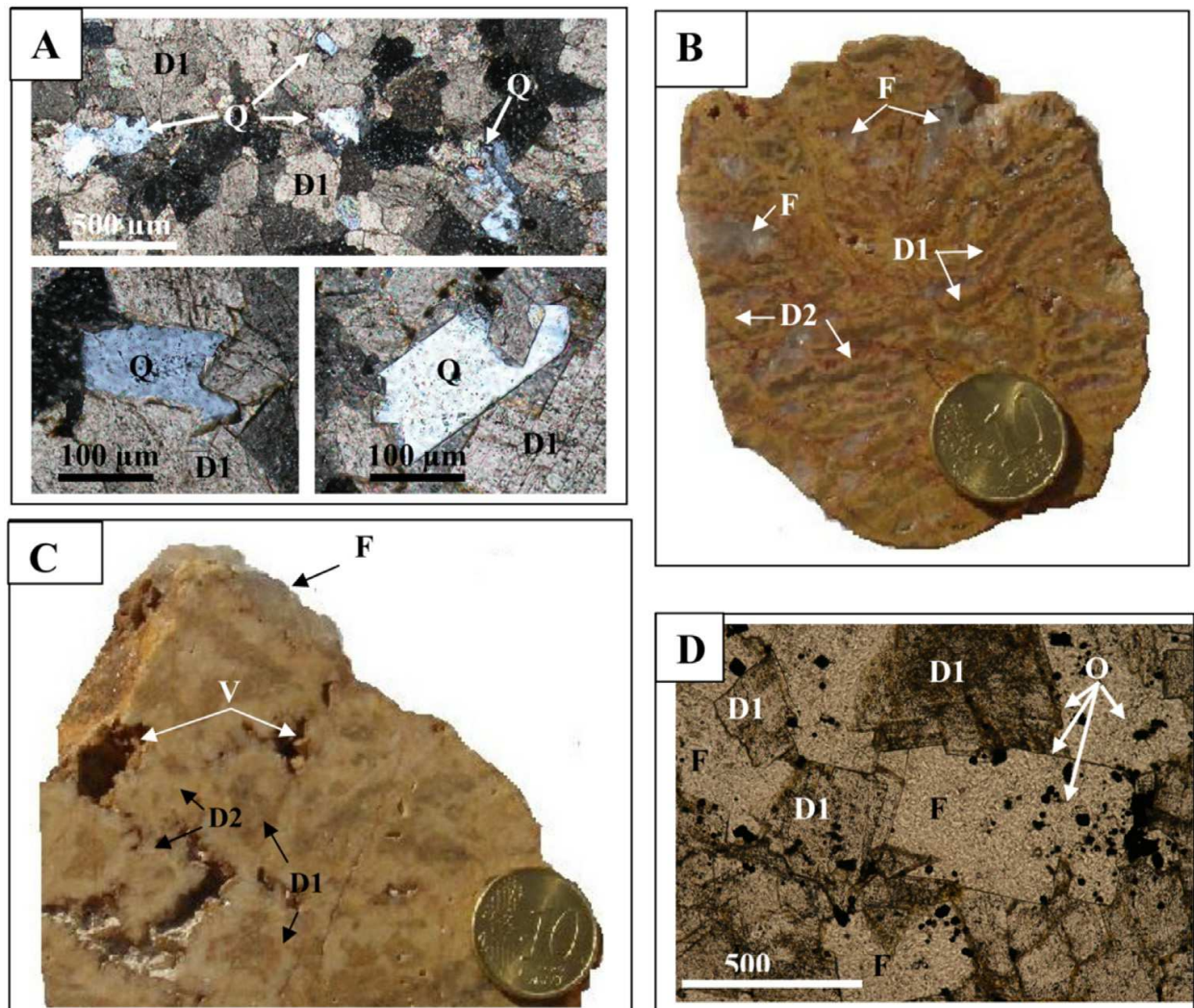


Fig. 7. Petrography of the dolomitized country rocks of the Hettangian-Lower Sinemurian. (A) Equigranular dolosparite (D1) with authigenic quartz (Q) remains (thin section, sample L6-31, crossed polars). (B) Banded dolosparite showing an alternation of dark dolosparite layers (D1) and recrystallized light-coloured dolomacrosparite (D2). Open spaces are filled with colourless fluorite (F), (sample C5-Dr), (C) Dolomitic breccia showing dark elements made of dolosparite (D1) cemented by a light-coloured dolomacrosparite (D2). Note the presence of open spaces (V), some of which are filled with colourless fluorite (F), (sample C5-Db), (D) Microfacies of the massive, mineralized dolostone; the matrix consists of a homogeneous dolosparite (D1) replaced by fluorite (F), (thin section, sample L3-22, polarized light).

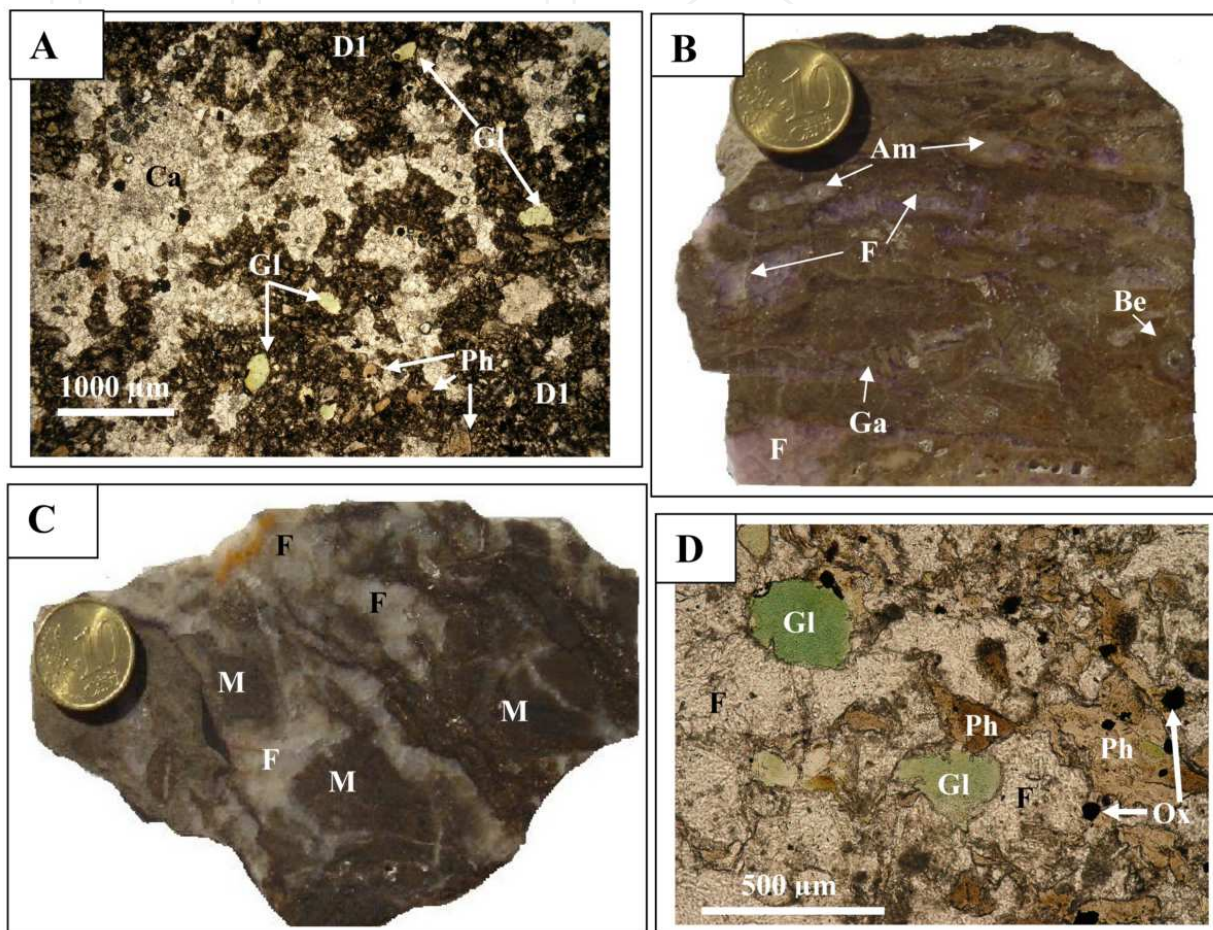


Fig. 8. Petrography of the Carixian facies. (A) Carixian phosphatic limestone affected by epigenetic dolomitization. Ferruginous dolosparite (D1) includes remains of glauconite (Gl) and phosphate (Ph) grains and is invaded by a late calcitization (Ca), (thin section, sample CC6-90, polarized light); (B) Fossiliferous limestone, rich in ammonites (Am), gastropods (Ga) and belemnite rostra (Be) filled with internal phosphatic cement. Macrogranular purple fluorite (F) has replaced part of the phosphate-carbonate matrix, epigenized fossil shells (Ga, Be) and filled the interiors of others (Am), (C) Brecciated facies of the phosphatic limestone showing elements of the matrix (M) cemented by a white macrogranular fluorite (F); (D) Detail from (C) showing the matrix (M) strongly replaced by fluorite (F). Only remains of phosphate (Ph), glauconite (Gl) grains and oxides (Ox) are preserved (thin section, sample JS1-6, slightly-crossed polars).

Petrographic group	Lithology / Ore facies / orebody	Age of layer/ore-bearing layer(s)	Sample	Petrographic description [Number of the old extraction open pit, as indicated in Fig. 3]	Petrographic type of fluorite	Mineralogy
I: Limestone and authigenic quartz	Backreef limestones	Lower Sinemurian	L6-5	Grey limestones [6]	-	Calcite
			L6-30	Grey limestones with authigenic quartz [6]	-	Calcite, quartz
			L6-30Q	Authigenic quartz [6]	-	Quartz
			L5-3	Massive yellow dolosparite [5]	-	
			DZ6-G	Grey dolosparite of the pseudo-brecciated facies (Fig. 7c) [6]	-	Dolomite
II: Dolostones and associated fluorite	Dolostones (Upper part of the Oust Formation)	Lower Sinemurian	DZ6-J	White sparry dolosparite of antipolar growth of the pseudo-brecciated facies (Fig. 7c) [6]	-	
			DZ6-F	Colourless fluorite filling voids in the pseudo-brecciated dolostone facies (Fig. 7c) [6]	Fl3	Fluorite
			JS1-6P	Nodular grey phosphate [1]	-	Apatite, calcite
III: Phosphatic limestone and associated fluorite	Phosphatic limestone Macrocrystalline fluorite associated with the phosphatic limestone	Lower Sinemurian	CC3-3	Macrogranular purple fluorite (Fig. 8b) [3]	Fl1b	Fluorite
			CC3-2	Macrogranular purple fluorite (Fig. 8b) [3]		
			JS1-6F	Macrogranular white fluorite (Fig. 8c) [1]		
IV: Finely-laminated dolostones and associated fluorite	Finely laminated karst deposits	Carixian	L3-21D	Dolomicrite (Fig. 9a,c) [3]	-	Dolomite, quartz ^s
			L3-21F	Microgranular fluorite replacing the carbonated matrix (Fig. 9a,c) [3]		Fluorite, dolomite ^s quartz ^m
			L5-16	Microgranular black fluorite with remains of matrix (Fig. 10a,b) [5]	Fl1a	
			L5-15F	Microgranular fluorite rich in matrix remains (Fig. 10c) [5]		Fluorite, quartz ^s , dolomite ^s , calcite ^s , apatite ^m
			L5-15G	Mesogranular-purple fluorite layers alternating with sample L5-15F [5]	Fl1b	
V: Banded ore		Carixian	FZ-5N	Microgranular fluorite with matrix remains (Fig. 11a,b) [5]	Fl1a	
			FZ-5B	Macrogranular-white fluorite (Fig. 11a,c) [5]	Fl1b	Fluorite, quartz ^s
VI: Megacrystalline fluorite and calcite in lodes		Sinemurian to Lower Toarcian	JS5-F	Cm-sized fluorite crystals [5, 6]	Fl2	Fluorite
			JS6-F	Cm-sized fluorite crystals [5, 6]		
			JS5-C	Cm- to dm-sized rhombohedral calcite crystals [5, 6]	-	Calcite
			JS6-C	Cm- to dm-sized rhombohedral calcite crystals [5, 6]		
VII: Fluorite in cavities	Intradolomitic pockets filled with residual clays Geode	Lower Sinemurian Carixian	L4-2	Cm- to dm-sized, cubic blue and purple fluorite [4]	Fl3	Fluorite
			JS3-5	Cm-sized cubic fluorite [3]		

Table 1. Samples selected for the MTE, REE and isotopic Sr geochemistry in the different petrographic facies of the wallrocks and the fluorite ore of Jebel Stah (s: secondary mineral phase, m: minor mineral phase).

as diffused clusters or lenticular bodies, resulting from the replacement of the carbonated matrix in the dolomitized horizon at the top of the Oust Formation (Fig. 7D), in the Carixian phosphatic layer (Fig. 8B-D) and in the intrakarst, finely-laminated deposits (Fig. 9). They contain relict dolomite, calcite, together with, apatite, glauconite and authigenic quartz, with rare sphalerite, galena and pyrite.

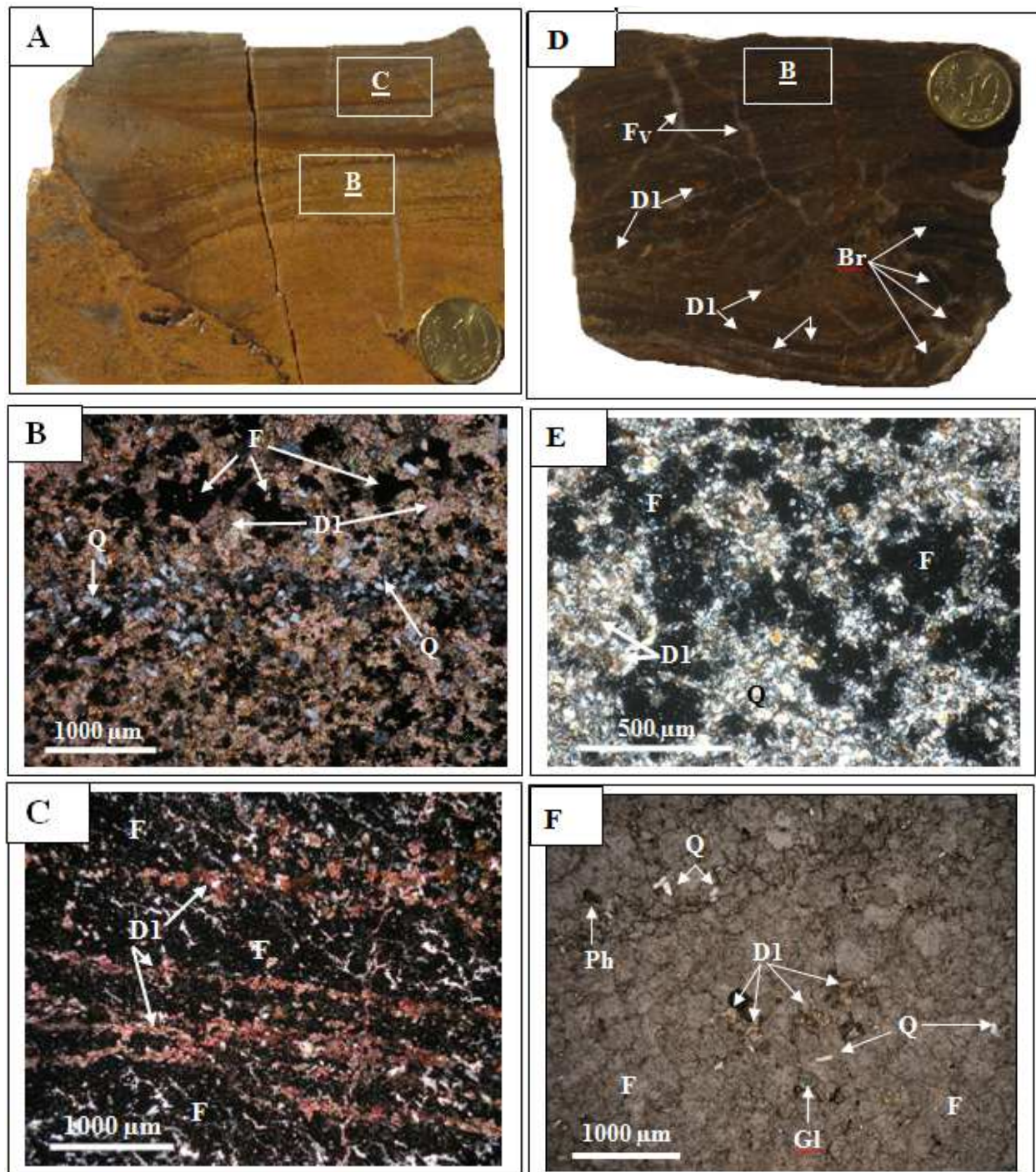


Fig. 9. Petrography of the fluorite-bearing Carixian facies. (A) Finely-laminated sediment filling a karst cavity at the top of the Hettangian-Lower Sinemurian, affected by epigenetic dolomitization (light grey laminae) and subsequent fluoritization (dark grey laminae), (Sample

L3-21, see B and C). (B) Strong dolomitization (D1) has affected the sediment in the lower part of the karst, only authigenic quartz (Q) in thin layers remains as a former sediment. Part of the dolomitic matrix has been replaced by fluorite (F), (thin section, crossed polars). (C) Dolomitic matrix (D1) at the top of the cavity, including remaining quartz crystals is replaced by a microgranular fluorite (F) rich in interstitial silica (thin section, crossed polars). (D) Finely-laminated dark sediment filling a karst cavity at the top of the Hettangian-Lower Sinemurian, including a sedimentary breccia (Br) wholly replaced by fluorite. The latter is evidenced macroscopically by light-coloured fluorite occurring as veinlets (F_V) and thin layers (F_L). Remains of the former matrix consist of only small yellow patches of dolomite (D1), (sample L5-16); (E) Details of the area delineated in A: the replacement of the former matrix by fluorite is almost total. Only small dolomitic patches (D1), quartz crystals (Q), phosphate (Ph) and glauconite (Gl) grains are preserved (thin section, sample L5-16, slightly crossed polars). (F) Details of a finely-laminated sediment filling a karst cavity at the top of the Hettangian-Lower Sinemurian, showing small patches of fluorite (F) replacing part of the matrix. This one is made of abundant authigenic quartz microcrystals (Q) with some dolomitic (D1) remains (thin section, sample L5-15, polarized light).

F11b. White-to-purple macrogranular fluorite, resulting from the recrystallization of the early fluorite generation (F11a) along the Carixian layer (Fig. 8B, C). Sometimes, the recrystallization gives rise to stratabound-banded structures which consist of an alternation of mm- to cm-scale dark layers of early fluorite and white layers consisting of a macrocrystalline fluorite of antipolar growth. Interstitial silica may be observed in either the microgranular (Fig. 9C) or the macrogranular fluorite-bearing layers.

F12. Large open-space fillings within vertical to sub-vertical extensional faults trending N030°-060°E and N090-130°E, and crosscutting the entire Liassic series, including the hanging wall Toarcian marls (Fig. 5). Fluorite consists of cm-sized colourless or white-to-yellowish crystals accompanied by calcite occurring as cm- to dm-sized white-to-pink rhombohedra.

F13. Colourless, white or purple fluorite occurring as small open space fillings (Fig. 7B, C) or as cm-to-dm-scale cubic crystals within large solution cavities either at the top of the Lower Liassic formation or within the Carixian layer.

4. Sampling and analytical methods

The microthermometric analyses were conducted with a "Chaixmeca" heating-freezing stage microscope which allows temperature measurements within the range -196 to +600 °C (Poty et al., 1976). Pure CO₂ and pure water specimens were used for calibration. The precision of temperature measurements is of the order of ±1 °C for the final melting temperatures (T_m) and the homogenization temperatures (T_h) in the -100 °C to +250 °C interval.

The crush-leach method (Roedder 1984) was used to collect the fluids contained in the inclusions (cf. Ames 1955; Hall and Friedman 1963; Roedder 1963, 1967, 1979; Sawkins 1968; Grappin et al. 1979; Deloule 1982). Fluorite samples were crushed in distilled water to extract the fluid trapped in the inclusions. The solids were then washed with distilled water. In order to separate the fluids contained in the inclusions of different generations, a large number of chips containing mainly primary, pseudosecondary, or secondary inclusions, are

selected by microscopic observations. The recovered solutions are analyzed for Na⁺, K⁺ by flame photometry (iso Bio type PHF 90D), Ca²⁺, Mg²⁺ by atomic absorption (Perkin Elmer Zeeman 5000) and F⁻, Cl⁻ and SO₄²⁻ by ionic chromatography (Dionex 2000i). There was a mean analytical error of 5% for all methods.

The geochemical characterization of fluorite was based on analysis for metallic trace elements (MTE), REE and Sr isotopes. Limestone (2 samples), authigenic quartz (1 sample), dolostone (4 samples) and phosphates (1 sample) from the wallrocks, along with samples representing the different petrographic facies and bodies of the fluorite ore at Jebel Stah (14 samples) have been collected from geological outcrop in the different open pits (Fig. 3; Table 1). Each has been described in the field, in hand specimen and in thin section. Prior to crushing, the broken samples were investigated and sub-divided under a binocular microscope to separate the different petrographic phases: carbonates, phosphates, microgranular "impure" fluorite including matrix remains (dolomite, silica, phosphate, clayey fraction) and macrogranular "pure" fluorite.

For the MTE and the REE determinations, 0.1 g of each powdered sample was dissolved in 0.5/0.6 ml HF/HNO₃ within a sealed teflon backer (savillex). After evaporation at 50 °C on a heating plate for 12 hours, the sample is redissolved in twice-distilled HNO₃ (2.8 ml) on the heating plate (sealed backer) for 24 hours. After dilution in 100 g of twice-distilled water (solution 1), 250 µl of ultrapure H₂O₂ (for the complexation of the Ta, to prevent its complexation by the REE) and 100 mg of powdered boric acid (to keep fluoride in solution by complexation), are added to the solution. The fluorite is completely dissolved by heating for 24 hours at 60 °C (solution 1). MTE and REE analysis was undertaken with an ICP-MS (type Elan 5000-Perkin Elmer). The standard limestone "CAL-S" (CRPG standard limestone; Potts et al., 2000) was used for calibration. Measurement reproducibility was better than 5 % relative for all elements.

For the Sr isotopic determinations, 1 ml of solution 1, was evaporated overnight at 50 °C. The residue was re-dissolved in 1 ml 6N HCl. A blank was prepared at the same conditions. Strontium was separated from the solutions using ion exchange columns. The ⁸⁷Sr/⁸⁶Sr ratio was measured on a 7-collector Finnigan MAT 262 thermal ionization mass spectrometer. Reproducibility of this ratio among replicate samples was always to an uncertainty below 0.000005 (2σ). Measured blanks for the procedure are negligible, yielding uncertainties significantly lower than reproducibility. The average value for the NBS 987 standard was ⁸⁷Sr/⁸⁶Sr = 0.710242 ± 0.000005 (2σ).

5. Fluid inclusions

5.1 Description of fluid inclusions

The studied fluid inclusions occurred in fluorites and in the massive quartz from Jebel Stah. Primary, pseudosecondary and secondary inclusions were recognized by microscopic observations of thin cleavage splinters.

5.1.1 The primary and pseudosecondary inclusions

These are up to 500 µm in size and often take the shape of negative crystals. Two types are observed:

- *Two-phase liquid-vapor aqueous (L+V type) inclusions* at room temperature, visible within the fluorite crystals of Jebel Stah. Some of these samples show trapped dolomite crystals. The liquid phase accounts for 95% of the inclusion volume. The initial melting temperature is about -50 °C, which is clearly lower than the eutectic temperature of the NaCl-H₂O system (-20.8 °C). This indicates the presence of bivalent cations such as Mg²⁺ and Ca²⁺ (Crawford 1981; Roedder 1984).

The salinity (S) of the fluids was obtained from the final melting temperatures of ice (T_m). The homogenization temperatures (Th) are measured during heating runs; all of the inclusions homogenize in the liquid state. The mean salinity ranges between 18 and 22.5 wt % NaCl equivalents for the early fluorites (F11b and F12). The homogenization temperatures range from 120 to 160 °C. Type 3 fluorite (F13) is characterized by medium salinity (10 wt % NaCl equivalents) and a higher mean Th range (175-180 °C). The inclusions contained in the quartz samples are characterized by low salinities of 5.5 wt% NaCl equivalents and homogenize in the range of 205-215 °C.

- *Two-phase gaseous CO₂-rich inclusions (L+V+CO₂G type)* within the massive quartz of Jebel Stah with variable phase ratios (50-95% liquid content). These inclusions freeze between -90 and -100 °C. Melting of solid CO₂ starts between -92 and -95 °C; mean final melting temperature (T_mCO₂) is -57.1 °C, which is lower than the eutectic temperature of pure CO₂ (-56.6 °C). The homogenization occurs in the gaseous state at a mean temperature (ThCO₂) of 19 °C. The density of CO₂ (0.19) was deduced from the relationship between the temperature of homogenization (ThCO₂) and the density of the CO₂ phase (Valakovich and Altunin, 1968, in: Shepherd et al., 1985).

5.1.2 Secondary inclusions

Two types of secondary inclusions were observed:

- Two-phase (L + V) aqueous fluid inclusions. The liquid phase fills up to 95% of the inclusion volume. The homogenization temperatures range between 140 and 200 °C. The salinities are low (3-6 wt% NaCl equivalents).
- Three-phase (L + P + V type) aqueous inclusions containing a droplet of petroleum (P) and visible in the large cubic fluorite crystals of Jebel Stah (F13).

5.2 The microthermometric results

The results of the microthermometric analyses are summarized in Table 2, where the final melting temperature of ice (T_m) and the homogenization temperature (Th) are given by their mean values. These are deduced by statistical analysis from histograms (symmetric distribution in most cases) constructed with a 10 °C interval for Th and T_mNaCl and 0.5 °C interval for T_m. More than 75 % of the temperature values lie in the modal value ±15 °C interval for Th and in the modal value ±0.75 °C interval for T_m. Finally, mean T_m and Th values are accepted with an error equivalent to the standard deviation interval, e.g. ±1 °C for T_m and ±5 °C for Th. The mean homogenization temperatures and salinities are translated in a Th Vs S plot (Fig. 10).

The fluorites F11 and F12 from Jebel Stah are characterized by similar mean homogenization temperatures and salinities that are, for the most part, clustered around 130 ± 5 °C and 19.5 ±

Sample	Sample description (Petrographic type)	Generation and composition of inclusions	Size (μm)	N	T _m \pm 1 ($^{\circ}\text{C}$)	Salinity \pm 1	
						(wt% NaCl equivalent s)	Th \pm 5 ($^{\circ}\text{C}$)
JSF-D	Fluorite in fine aggregates replacing dolomite (F11a)	Primary L+V	10-50	26	-20	22.5	120
L6-1	Fluorite filling voids in the dolomite (F11b)	Primary L+V	20-200	16	-14	18	125
CC5	Fluorite in fine aggregates	Primary L+V	20-100	24	-16	19.5	145
CC5-51	replacing carbonates of the			7			
CC4-41	karstic deposits (F11a)			8			
JS1-6	Massive fluorite filling voids in the phosphatic carbonates (F11b)	Primary L+V	10-100	23	-17	21	130
L3	Massive fluorite of the banded ore (F11b)	Primary L+V	10-100	25	-16	19.5	150
JS3-8	White sparitic fluorite of the intradolomitic karstic druses (F12)	Primary L+V	50-300	25	-15	19	125
		Pseudosecondary L+V	10-50	32	-15	19	120
JS3-5	White fluorite of the intradolomitic geodes (F12)	Primary L+V	50-500	25	-16	19.5	160
		Pseudosecondary L+V	50-200	35	-16	19.5	125
JS1-5	White fluorite of the intradolomitic geodes (F13)	Primary L+V	50-500	26	-6.5	10	180
		Pseudosecondary L+V	10-50	32	-6	9.5	140
		Secondary L+V+P	50-500	21	-	-	115
L4-2	Macrocrystalline fluorite associated with marly intradolomitic dissolution druses (F13)	Primary L+V	100-700	32	-6.5	10	175
CC1-3	Purple sparitic fluorite of the intradolomitic karstic druses (F13)	Primary L+V	100-500	24	-6.5	10	175
		Secondary L+V+P	10-50	28	-2	4	200
JS1-14	Massive quartz from the intradolomitic fractures	Primary L+V	50-400	42	-3	5.5	215
		Pseudosecondary L+V	10-100	25	-3	5.5	205
		Primary and pseudosecondary CO ₂ gas	20-200	20	-57.1	-	19*

Table 2. Sample description, generation and composition of inclusions and microthermometric results of the fluid inclusions in the fluorites and the quartz of Jebel Stah. N number of inclusions, T_m ice melting temperature, Th homogenization temperature, L aqueous liquid, V aqueous vapor.

1 wt% NaCl equivalents, respectively (Fig. 10, Table 2). The deposition of the fluorite F13, followed by the massive quartz, is accompanied by an increase in temperature (mean T_h = 175 \pm 5 $^{\circ}\text{C}$ and 207 \pm 5 $^{\circ}\text{C}$) and a decrease in the mean salinity (10 \pm 1 wt % NaCl equivalents and 5.5 \pm 1 wt % NaCl equivalents; Fig. 10, Table 2). These figures, show that the fluorites F11 and F12 (types 1 and 2) belong to the first generation. Field observations alone did not allow this distinction. Consequently, the vertical faults (Fig. 3) should be the drain that channelled the ascending hydrothermal ore fluids that deposited the fluorite F12 within the large dissolution cavities superimposed to the faults near the unconformity surface. The fluids infiltrated horizontally through the porous rocks of the Lower-Middle Liassic allowing the replacement of the carbonate substratum and giving rise to fluorite F11. The

fluorite F13 corresponds to a second generation, which crystallized later in large, well-shaped cubic crystals within geodes.

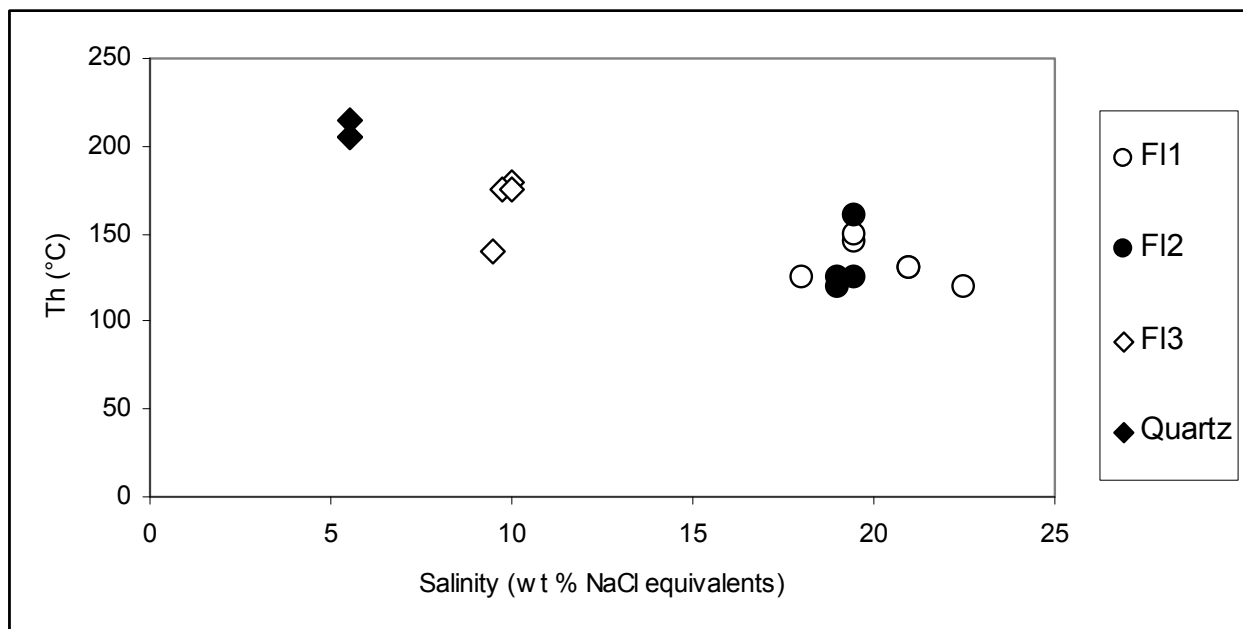


Fig. 10. Mean homogenization temperature versus mean salinity of primary and pseudosecondary aqueous fluid inclusions in fluorite and massive quartz from Jebel Stah.

The fluids trapped either within the secondary inclusions of fluorite or within the primary and pseudosecondary inclusions of the massive quartz of Jebel Stah are characterized by the lowest salinities ($3-6 \pm 1$ wt % NaCl equivalents), and mean homogenization temperatures ranging from 140 ± 10 °C to 200 ± 10 °C as well as the presence of gaseous CO₂. These observations strongly suggest the presence of fluids rich in gaseous CO₂ which permeate at a late stage the Jebel Stah and give rise to the massive quartz. Perthuisot (1978) and Perthuisot et al. (1978) also documented the presence of CO₂-rich fluids associated with diapirism in northern Tunisia. At Hammam Zriba, earlier microthermometric studies of the inclusions occurring in the fluorite (Bouhlef 1982; Bouhlef et al. 1988) also indicated a homogenization temperature increase from 100 to 185 °C from the first to the third fluorite generation.

5.3 Temperatures of formation (T_f) of host minerals

The formation temperature (T_f) of a mineral is equal to, or higher than, the homogenization temperature (T_h) of its primary or pseudosecondary inclusions. It may be given by: $T_f = T_h + \Delta T$, where ΔT is the pressure correction (Roedder 1979, 1984). Bouhlef et al. (1988) suggested a $\Delta T \leq 20$ °C for the aqueous inclusions of the fluorite from Hammam Zriba hosted at the top of the Jurassic series, and proposed $T_f = (T_h + 10 \text{ °C}) \pm 10 \text{ °C}$ as a relation including all the possible temperature correction values in the 0-20 °C interval. The geologic setting allows us to work with $\Delta T \leq 30$ °C (Potter and Calif 1977) for the mineralizations of Jebel Stah, hosted in the Lower Jurassic series.

Stretching has to be considered for the fluorite samples formed under the lower temperature conditions, e.g. the fluorites F11 and F12 (Fig. 10, Table 2). The consequent overheating is

estimated to be caused by temperatures approaching the crystallization temperature of the Jebel Stah massive quartz. In such conditions, the fluorites Fl1 and Fl2 have undergone an overheating of 80 ± 10 °C, while the fluorite Fl3 has undergone a lower overheating of 35 ± 10 °C. The mean Th values ($Th \pm 5$ °C) should be lowered by a ΔTh (amount of stretching, Bodnar and Bethke, 1984) of about -10 °C for the fluorites Fl1 and Fl2 and -5 °C for the fluorite Fl3. The fluid inclusions of the massive quartz as well as the secondary inclusions are supposed not to be subjected to significant overheating, to stretch.

Taking into account the errors on Th rising from both of the statistical analysis (± 5 °C), and the stretching ($-\Delta Th$), the relation given by Bouhlef et al. (1988) becomes: $Tf = \{(Th - \Delta Th + \Delta T/2) \pm (5 + \Delta T/2)\}$ °C. It follows that the mean formation temperatures will be (Table 3): 135 ± 20 °C for the fluorites Fl1 and Fl2, 185 ± 20 °C for the fluorite Fl3 and 225 ± 20 °C for the massive quartz.

Mineral	Petrographic type	$T_m \pm 1$ (°C)	Salinity ± 1 (wt % NaCl equivalents)	$Th \pm 5$ (°C)	Generation	Overheating ± 10 (°C)	ΔTh (°C)	$Tf \pm 20$ (°C)
Fluorite	Fl1a, b	-16.5	20	130	I	80	-10	135
	Fl2	-15.5	19	130				
	Fl3	-6.5	10	175	II	35	-5	185
Quartz	-	-3	5.5	210	-	-	0	225

Table 3. Average final melting temperatures (T_m), salinities, and homogenization temperatures (Th) deduced from microthermometric analyses, fluorite generations, and formation temperatures (Tf) of primary and pseudosecondary fluid inclusions in fluorite and massive quartz of Jebel Stah.

6. Composition of the ore fluid

The analytical results are reported in Table 4. The measured concentration values depend on the dilution factors related to the washing process and cannot be compared from one sample to another. The dilution factors are estimated by comparing the salinity values deduced from the microthermometric measurements (Table 2) and chemical analysis (Weisbrod and Poty 1975). They range between 6.10^3 and 10^5 . The calcium concentration in the inclusions (Ca^*) was calculated by subtracting from the measured value the quantity of Ca resulting from fluorite dissolution during the aqueous crushing and rinsing. Fluorite dissolution was estimated from fluoride concentration in the leachates. Fluorite solubility is about $0.3 \cdot 10^{-3}$ mol/kgH₂O in a 2-4 M NaCl solution at 25°C (Strubel 1965). Taking into account the dilution, fluorite concentrations in the leachates should not exceed 10^{-7} mol/l, if fluorite dissolution did not occur during the aqueous crushing and rinsing, but the observed values were higher than 0.17 mol/l. Therefore, the fluoride concentration in the leachates can be attributed essentially to fluorite dissolution during the extraction run (within an error lower than 0.1%).

The molar ratios Cl/Na, Mg/Na, Ca/Na and SO₄/Cl, calculated from the ionic concentrations (Table 4), show that the ore-forming fluids are sodium-calcium-chloride brines. Fig. 11 shows the variations of these molar ratios versus the salinity of the solutions. The inclusions in the fluorites of the first generation (Fl1 and Fl2) result from highly saline (20 ± 1 wt % NaCl equivalents) and Na-rich fluids. They exhibit comparable molar ratios for all the major elements.

Fluorite type	Sample (Inclusion generation)	Salinity (wt% NaCl equiv.)	Concentrations in leachates mol/1 X10 ⁵							Charge balance Δ epm%	Molarity				Temperature ($\pm 25^\circ\text{C}$)	
			Na ⁺	K ⁺	Mg ⁺⁺	Ca ⁺⁺	Cl ⁻	SO ₄ ⁻⁻	F ⁻		Na	K	Ca*	Mg	Na-K	Na-K-Ca
1	JS1-6 (P)	21	20	2.6	0.5	22.7	19.3	0.9	46.75	1	3.1	0.4	-	0.08	310	-
3	JS1-5 (P)	10	3.6	0.7	0.28	19.7	5	0.3	36	3.2	0.95	0.2	0.45	0.06	380	300
3	CC1-3 (P)	10	2.2	0.4	-	-	2.6	-	-	0.2	-	-	-	-	270	-
3	L4-2 (P)	10	4.6	1	0.4	19.3	5.8	0.6	35.7	2.8	1	0.22	0.34	0.09	390	310
2	JS3-8 (PS)	19	5.4	0.75	0.2	15.7	5.5	0.3	29.3	3.7	3	0.43	0.6	0.1	300	300
3	JS1-5 (PS)	9.5	2.5	0.25	0.2	9.6	3.6	0.4	17	2.2	0.95	0.09	0.42	0.07	260	240
3	CC1-3 (S)	4	4.6	0.5	0.25	17.4	10.6	0.5	31.9	-3.6	0.45	0.04	0.14	0.02	270	240

Table 4. Chemical composition and molar ratios in the inclusion fluids recovered after the washing in the inclusions; calculated Na, K, Ca and Mg molar concentrations and estimated reservoir temperatures from the Na, K, Ca concentrations in the fluorite fluid inclusions. (Ca* = Ca total - Ca associated to fluoride, see text).

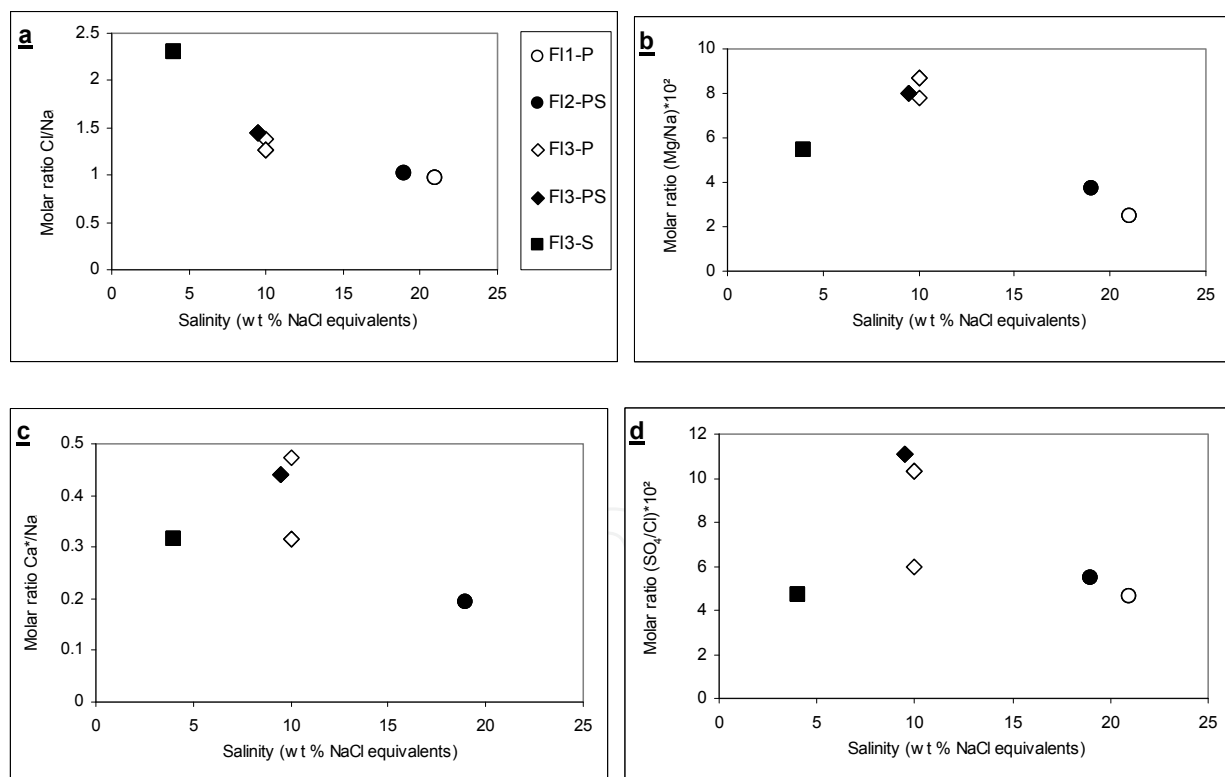


Fig. 11. a-d: Plot of the molar ratios Cl/Na, Mg/Na, Ca*/Na and SO₄/Cl versus the salinity in the extracted inclusion fluids from the fluorites of Jebel Stah (Ca* = Ca total - Ca associated to fluoride, see text and table 4).

The inclusion fluid of the second fluorite generation (F13) is clearly distinct from that of the first generation: the Cl/Na molar ratio increases from 1 to 1.5 (Fig. 11a), Mg/Na increases

from $3 \cdot 10^{-2}$ to $8 \cdot 10^{-2}$ (Fig. 11b), Ca/Na increases from 0.25 to 0.45 (Fig. 11c) and SO_4/Cl increases from $5 \cdot 10^{-2}$ to $11 \cdot 10^{-2}$ (Fig. 11d). NaCl represents more than 90 mol% of the fluid salt content for the fluorites F11 and F12 and only 70 mol% for the Fluorite F13. Thus, the lowering of the salinity (10 ± 1 wt% NaCl equivalents) is accompanied by a relative increase in the concentration of the dissolved species other than NaCl (e.g. $CaCl_2$, $MgCl_2$). This confirms the generation of the Jebel Stah fluorite from two chemically distinct fluids and during two successive phases, as previously deduced from the microthermometric results (Fig. 10).

The calculated molarities of Na, K, Ca and Mg, taking account of the dilution, are reported in Table 4. Their variations are plotted in Fig. 12 as a function of the salinity of the fluids. The molarities exhibit linear correlation with salinity for all the cations. However, the molarity decrease observed for the late fluorite F13, is due to dilution of the highly saline and Na-rich fluid by mixing with warmer, less saline and Na-poor fluid in addition to its high Ca and Mg content. The latter fluid should be the one trapped in the secondary inclusions of the fluorite F13 (4 ± 1 wt% NaCl equivalents).

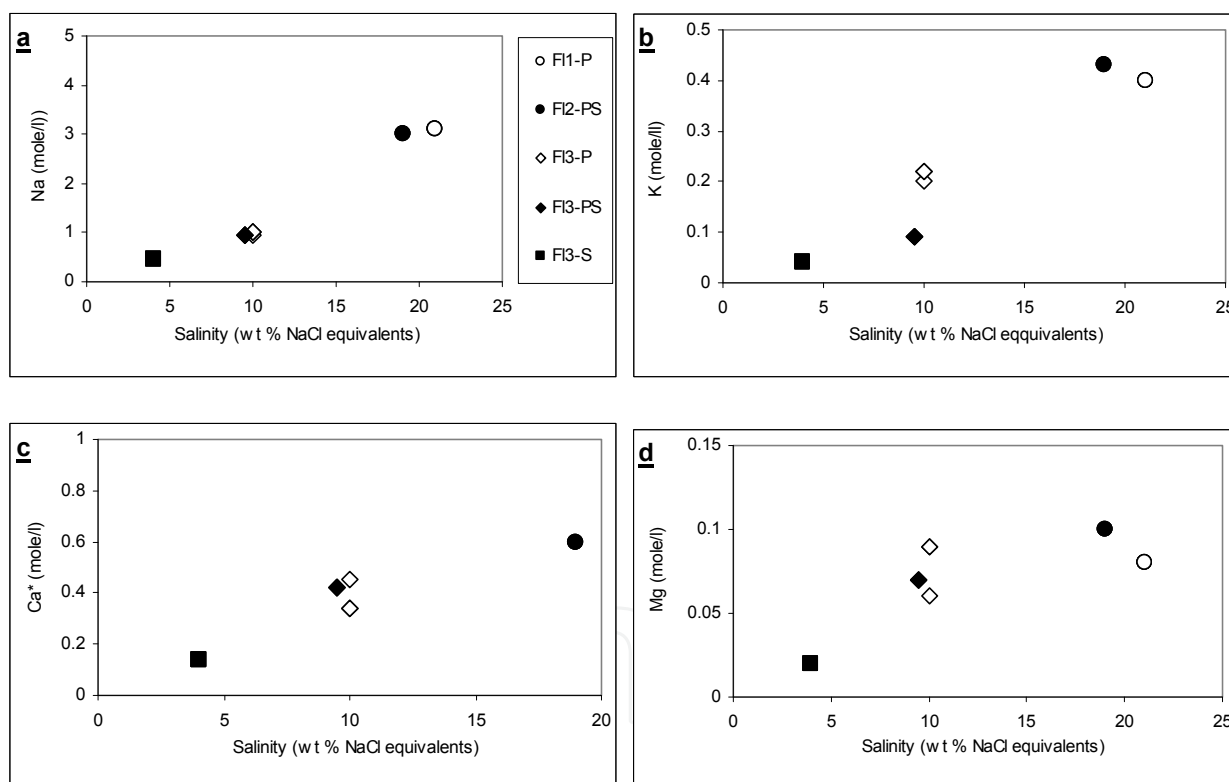


Fig. 12. a-d: Plot of the Na, K, Ca and Mg concentrations versus salinity in the extracted inclusion fluids from the fluorites of Jebel Stah ($Ca^* = Ca$ total - Ca associated to fluoride, see text and table 4).

7. Estimation of the reservoir temperature

Relations between the reservoir temperature and the chemical composition of hydrothermal fluids have been established from studies dealing with present geothermal sources (Ellis

1970; Fournier and Trusdell 1973). Fournier and Trusdell (1973) have shown that the results can be extended to the fluids contained in fluid inclusions.

The “Na-K” geothermometer presupposes the equilibrium between the fluid and Na-K feldspars. The temperature of the fluid is related to the Na/K ratio by: $T = [908/\log(\text{Na}/\text{K}) + 0.7] - 273.15$; where T is expressed in °C and the concentrations in mol/l. This relation can be used for the Ca-poor alkaline solutions close to neutrality (Ellis 1970). The temperatures calculated from this equation are listed in Table 4. They are generally close to 275 ± 25 °C; the uncertainty, due to the analytical errors on Na, K and Ca, averages 10% and is nearly equal to the mean deviation from the mean temperature value.

The “Na-K-Ca” geothermometer (Fournier and Trusdell 1973) can be applied to Ca-rich solutions. The temperature of the fluid is expressed by: $T = [1647((\log \text{Na}/\text{K} + 1/3 \log(\text{Ca}/\text{Na})) + 2.24)] - 273.15$; (T in °C and concentration in mol/l). The temperatures calculated from this equation are listed in Table 4. They are consistent with the Na-K temperatures, with the exception of two samples (JS1-5 and L4-2), for which the $T_{\text{Na-K}}$ are anomalous and higher than the corresponding $T_{\text{Na-K-Ca}}$ values. These samples are characterized by the lowest Na/K ratios. On the other hand, post-Jurassic [Lower Cretaceous (Neocomian and Barremo-albian), Upper Cretaceous-Paleocene, Oligocene and Miocene] extensional phases are well documented in Tunisia (Turki 1988, Bagdasarian et al., 1972; Bouaziz et al., 2002). These phases induced the recurrent movement of the major faults (Zaghouan and associated faults) and thus hydraulic fracturing which favored the circulation of basinal fluids initially in contact with ante-Jurassic sediments.

8. Fluorite characterization

The selected host rock and fluorite ore samples (Table 1) were the objects of a geochemical study consisting of MTE, REE and Sr isotope analysis.

8.1 MTE geochemistry

In comparison to average concentrations of MTE in carbonates (Mason, 1966) and limestones (Rose et al., 1979), our results (Table 5, Fig. 13) show that no MTE anomalies are associated with the Lower Liassic wallrock limestones. In fact, they are even depleted in Mn, Ni, Ga, Rb, Th and U with respect to average concentrations in carbonates. The Carixian phosphatic limestones are depleted in Mn, but rich in Zn and Cd. Compared to Lower Liassic limestones, the dolomitic facies [massive (Fig. 7a), banded (Fig. 7b) or pseudo-brecciated (Fig. 7c)] are characterized by a distinct Zn anomaly and are rich in Mn.

Among the ore samples, only the microgranular fluorite of the finely-laminated karst deposits and the dark layers of the banded ore (early fluorite generation: F11a, Table 1) are anomalous in terms of Zn (101 to 409 ppm), Cd (0.7 to 13.5 ppm) and Pb (49 to 150 ppm). Indeed, all these sediments contain high proportions of phosphatic remains, as attested by the petrographic observations. However, obvious concentrations of U (29.7 ppm) and Rb (25.2 ppm) are observed only in sample L5-15F. The former should be justified by the

presence of phosphate remains (Prévôt et al., 1979), while the latter is due to the presence of a significant clay mineral fraction (Rose et al., 1979), as demonstrated by chemical analysis (3.4 wt.% Al₂O₃).

Fluorites of all other petrographic types (Fl1b, Fl2, Fl3; Table 1) are strongly depleted in all MTE, and particularly in Mn (≤ 0.1 ppm), and except for the high content in Co (13.4 to 40.5 ppm), and with respect to either the carbonate host-rocks (limestone, dolostone, phosphatic limestone) or the early fluorite facies (Fl1a). It is noteworthy, however, that in the subvertical lodes, a chemical fractionation of Mn and Co is observed between the megacrystalline fluorite (Fl2) and the coeval calcite: Mn permeating preferentially the lattice of calcite and Co that of fluorite.

	I			II				III			
	L6-5	L6-30	L6-30Q	L5-3	DZ6-G	DZ6-J	DZ6-F	JS1-6P	CC3-3	CC3-2	JS1-6F
Mn	61.5	58	11	158	534.4	572.5	0.43	1.6	0.12	0	0
Co	2	2	0.25	< d.l.	6.16	7.32	7.33	5.5	7.34	17	7.4
Ni	3	1.25	2	< d.l.	3.300	1.830	0.33	6.5	0.85	4.5	8
Cu	2	1.5	0.7	1	1.43	0.65	0.5	9	0.54	3	3
Zn	34	9	20.5	36	205	159.9	3.46	467	3.82	5.5	2
Ga	0.03	0.02	0.021	< dl	0.14	0.08	0	4.56	0.01	0.019	0.07
Rb	0.08	0.03	0.038	0.04	0.21	0.1	0.01	7.82	0.09	0.039	0.036
Mo	0	0.06	0.46	0.16	2.89	1.19	0.08	0.35	0.04	0.035	0
Cd	0.2	0.13	0.02	0.036	0.04	0.05	0	5.78	0.02	0.031	0.02
Ba	9	9	9.5	0.12	5.14	3.35	0.59	6	3.28	0.6	0.02
Pb	10.2	2.25	3	0.6	2.69	1.49	0.12	9.75	0.36	3.25	0.5
Th	0.009	0.02	0.049	0.007	0.05	0.02	0.01	1.32	0.13	0.118	0.033
U	0.459	0.27	0.08	0.326	0.21	0.1	0.004	4.98	0.11	0.028	0.012
La	0.384	0.35	0.068	0.17	0.56	0.21	0.01	4.354	0.12	0.068	0.076
Ce	0.47	0.42	0.109	0.24	0.73	0.3	0.01	4.717	0.2	0.122	0.144
Pr	0.09	0.08	0.019	0.034	0.11	0.06	0.0027	1.313	0.05	0.036	0.04
Nd	0.444	0.39	0.075	0.146	0.38	0.28	0.02	6.618	0.31	0.224	0.237
Sm	0.107	0.1	0.019	0.024	0.037	0.061	0.011	1.506	0.104	0.088	0.08
Eu	0.05	0.05	0.006	0.011	0.007	0.015	0.003	0.609	0.03	0.051	0.042
Gd	0.129	0.13	0.019	0.025	0.034	0.075	0.023	1.752	0.229	0.232	0.197
Tb	0.016	0.02	0.002	0.003	0.006	0.011	0.003	0.23	0.038	0.037	0.03
Dy	0.094	0.11	0.013	0.018	0.034	0.066	0.022	1.394	0.253	0.244	0.197
Ho	0.018	0.02	0.003	0.004	0.009	0.015	0.005	0.284	0.056	0.054	0.043
Er	0.054	0.06	0.007	0.013	0.031	0.047	0.01	0.744	0.154	0.146	0.114
Tm	0.007	0.01	0.001	0.001	0.005	0.007	0.001	0.085	0.017	0.016	0.012
Yb	0.037	0.05	0.006	0	0.04	0.055	0.002	0.262	0.091	0	0
Lu	0.006	0.01	0.001	0.001	0.007	0.01	2 ^E -04	0.064	0.012	0.012	0.009
ΣREE	1.91	1.8	0.35	0.69	1.99	1.212	0.12	23.9	1.66	1.33	1.221
⁸⁷ Sr/ ⁸⁶ Sr ±2σ						0.708180 ± 7				0.708613 ± 12	0.708154 ± 8

	IV					V		VI				VII		
	L3-21D	L3-21F	L5-16	L5-15F	L5-15G	FZ-5N	FZ-5B	JS5-F	JS6-HF	JS5-C	JS6-HC	L4-2	JS3-5	
Mn	184.9	15.96	50	19.9	227.9	19.6	0.75	0.09	0.103	152.1	156.1	0.029	0.04	
Co	2.53	5.15	6	10	5.85	5.09	13.4	14.56	40.49	2.88	11.9	7.723	30	
Ni	5.23	1.37	8.65	15.13	15.65	1.34	1.68	0.95	5.64	0.56	1.25	1.31	2.16	
Cu	5.09	5.27	6	13	4	10.23	0.65	0.463	1.16	0.248	0.56	0.701	1.16	
Zn	401	169	105	180	138	409	46.3	2.93	1.38	4.28	1.55	1.628	2.4	
Ga	0.05	0.048	1.173	6.16	1.71	1.52	0	0.005	0.003	0.006	0.03	0.006	0.005	
Rb	0.16	0.259	5.091	25.2	6.81	3.48	0.04	0.024	0.023	0.034	0.03	0.017	0.01	
Mo	1.16	0.347	0.39	1.82	0.9	0.86	0.05	0.085	0.058	0.118	0.11	0.169	0.22	
Cd	2.15	1.59	0.7	0.09	1.2	13.5	0.28	0.004	0.013	0.046	0.01	0.004	0.01	
Ba	12.08	2.71	7.5	33.9	29.8	248.4	1.48	1.73	1.35	1.26	0.57	2.298	5.17	
Pb	58.6	20.81	90	48.7	87.8	149.7	3.48	0.16	1.08	0.92	0.26	0.15	0.13	
Th	0.06	0.06	0.251	3.04	0.78	0.32	0.12	0.007	0.005	0.04	0.19	0.014	0.01	
U	0.21	0.19	1.12	29.7	5.71	0.64	0.06	0.001	0.001	0.05	0.09	0.001	0.002	
La	0.15	0.149	1.792	11.5	3.36	1.41	0.03	0.007	0.004	0.154	0.458	0.008	0.01	
Ce	0.22	0.256	2.32	14.8	4.23	1.95	0.07	0.02	0.012	0.73	1.83	0.017	0.01	
Pr	0.03	0.048	0.372	3.32	0.856	0.27	0.02	0.004	0.004	0.218	0.61	0.003	0.0032	
Nd	0.13	0.237	1.562	16.9	3.89	0.95	0.13	0.022	0.023	1.37	4.06	0.024	0.02	
Sm	0.028	0.057	0.249	4.79	0.946	0.15	0.051	0.014	0.012	0.54	2.14	0.01	0.015	
Eu	0.008	0.016	0.099	1.06	0.217	0.043	0.017	0.006	0.004	0.138	0.64	0.005	0.005	
Gd	0.044	0.106	0.302	5.18	1.09	0.202	0.129	0.029	0.032	0.62	2.92	0.021	0.035	
Tb	0.007	0.015	0.043	0.67	0.146	0.032	0.022	0.004	0.004	0.091	0.486	0.003	0.004	
Dy	0.045	0.1	0.272	3.47	0.766	0.218	0.153	0.024	0.019	0.491	2.59	0.014	0.024	
Ho	0.011	0.022	0.059	0.643	0.145	0.049	0.032	0.005	0.004	0.09	0.46	0.003	0.005	
Er	0.033	0.06	0.157	1.629	0.377	0.134	0.091	0.01	0.008	0.23	1.13	0.006	0.01	
Tm	0.004	0.006	0.018	0.19	0.043	0.016	0.009	0.001	0.001	0.028	0.129	4 ^E -04	0.001	
Yb	0.022	0.031	0	1.08	0.251	0.093	0.05	0.004	0.006	0.17	0.789	0.003	0.006	
Lu	0.003	0.004	0.015	0.163	0.035	0.013	0.006	0.001	0.001	0.022	0.109	5 ^E -04	0.001	
ΣREE	0.74	1.107	7.26	65.4	16.4	5.53	0.81	0.151	0.13	4.892	18.4	0.12	0.15	
⁸⁷ Sr/ ⁸⁶ Sr	0.708212					0.708333		0.708154		0.708280		0.708309		
±2σ	± 8					± 9		± 8		± 10		± 12		

Table 5. Results of the MTE, REE (ppm) and ⁸⁷Sr/⁸⁶Sr ratios analysis conducted on the country rocks and the different petrographic types of the fluorite ore of Jebel Stah. [Samples and petrographic groups (I to VII) are the same as in Table 1; <d.l.: values below the minimum detection limit (0.0075 ppm for Co and 0.366 ppm for Ni, NA: not analyzed)]

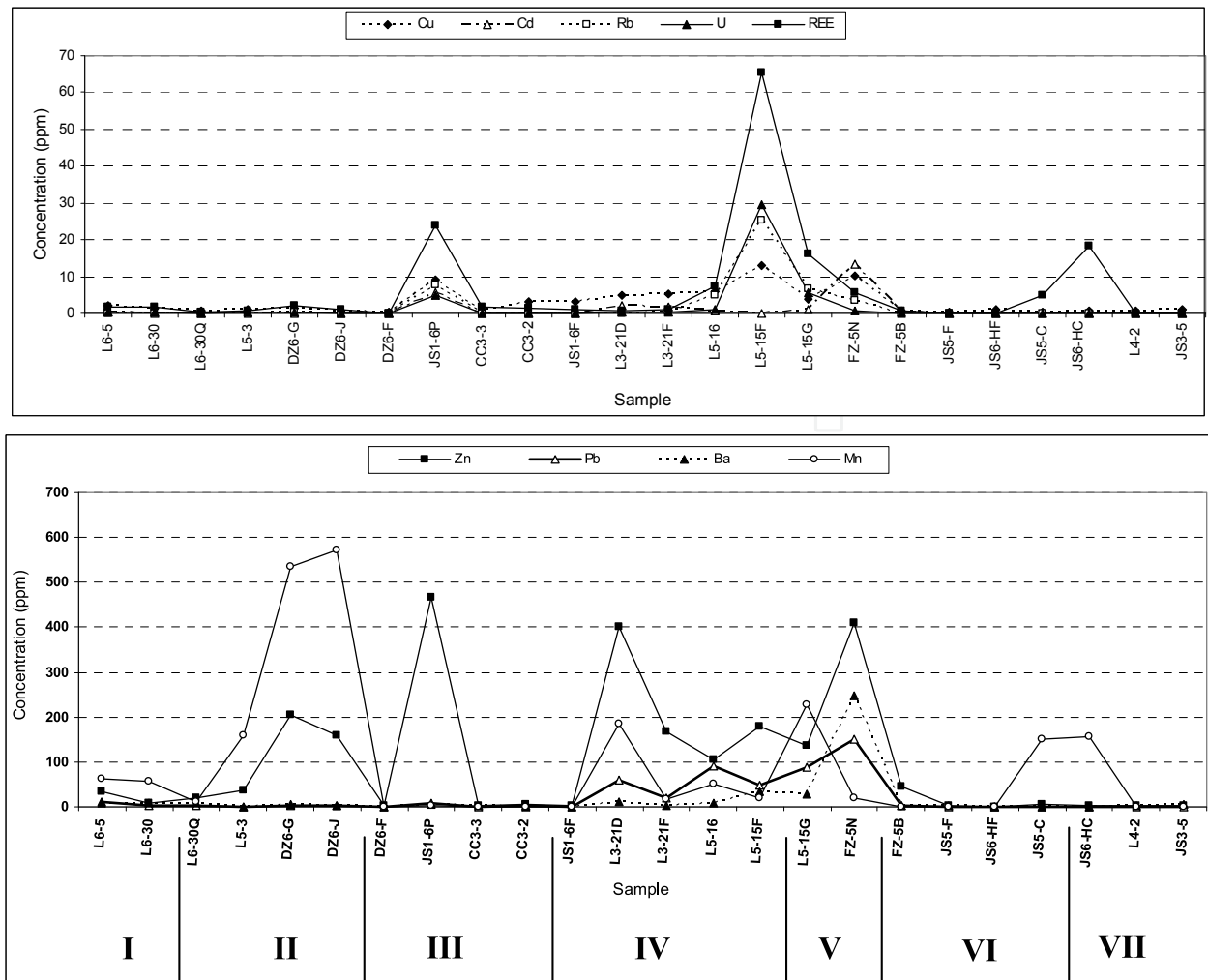


Fig. 13. Total rare earth element (REE) and MTE concentrations in the wallrocks and the different petrographic types of fluorite ore. Samples and petrographic groups I to VII are as in Table 1.

8.2 REE geochemistry

Due to its physico-chemical behaviour during the genesis of hydrothermal deposits, fluorite is one of the most important indicators of ore-forming processes in carbonate sediments (Schneider et al., 1975, 1977; Bau et al., 2003; Sallet et al., 2005). Fluorite is capable of fossilizing, with almost no deformation, thus preserving the lanthanide signature of the ore-forming solutions (Möller et al., 1984; Sallet et al., 2000; Schwinn and Markl, 2005). The results of REE analysis conducted on the wallrocks and the different fluorite-bearing facies are summarized in Table 5. The interpretation is based on the total REE content (\sum REE) and on the ratios between the different REE. REE patterns are normalized to chondrites according to Taylor and McLennan (1985).

The \sum REE values show differences according to the petrography and the mineralogy of the samples (Fig. 13). Among the wallrocks, carbonates (limestones and dolostones) are characterized by low \sum REE (0.35 to 2 ppm). Among the fluorite-bearing samples, those associated with the karst deposits (early fluorite ore; type F11a), are rich in REE (\sum REE = 7.25

to 65.4 ppm). The macrogranular fluorites, associated with Carixian deposits of type F12 (JS1-6F, CC3-2, CC3-3, FZ-5B) are characterized by $\sum\text{REE}$ values that are much lower (0.8 to 1.6 ppm) than those in the phosphatic limestones. The lowest $\sum\text{REE}$ values (0.12 to 0.15 ppm) are recorded in type F12 fluorites occurring within the vertical lodes (samples JS5-F, JS6-F), or in type F13 samples occurring within cavities (samples JS3-5, L4-2). The megacrystalline calcites in the vertical lodes (samples JS5-C, JS6-C), are characterized by $\sum\text{REE}$ values (5 to 18.35 ppm) higher than those in coeval fluorite.

Figure 14 shows that the chondrite-normalised REE patterns may be split into three groups:

- Wallrock limestones and phosphatic limestones (Fig. 14a) are characterized by “normal marine” patterns (gradual decrease from La to Lu), being slightly enriched in light REE (LREE) relative to heavy REE (HREE), along with a negative Ce anomaly. In addition, these signatures assume a specific shape due to a weak positive Eu anomaly superimposed onto all the REE patterns.
- Epigenetic dolomites (Fig. 14b) and microgranular fluorites of the type F11a (Fig. 14c) are characterized by REE patterns sloping to the right of the diagram. Such patterns are reminiscent of shales onto which small Ce and Eu anomalies are superimposed.
- Macrogranular fluorites belonging to the petrographic types F11b, F12 and F13 (Table 1). All the REE patterns display LREE depletion [$(\text{Tb}/\text{La})_{\text{N}} > 1$], in comparison with the other rock types above. The patterns also display weak Ce and Eu anomalies. The peak is centred on Sm-Gd for calcites and on Gd for fluorites.

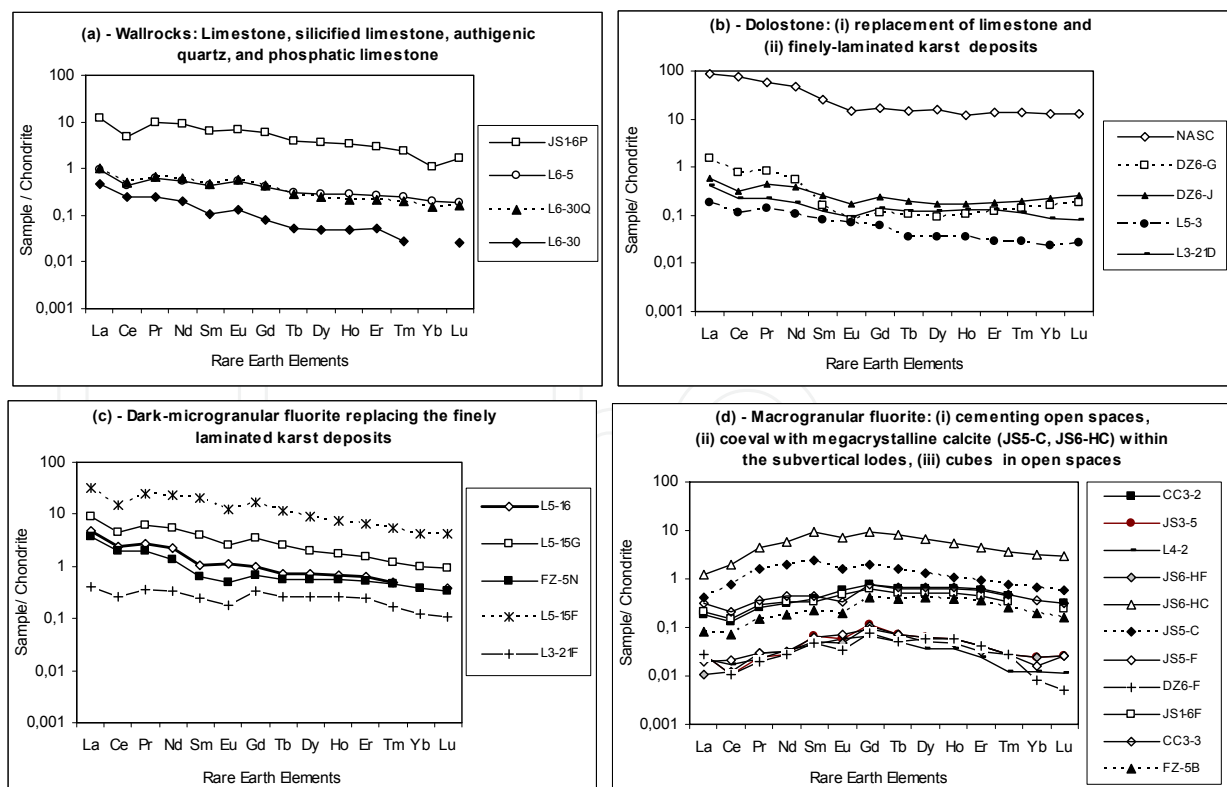


Fig. 14. REE spectra of the wallrocks (a, b) and the different petrographic types of fluorite (c, d). [REE abundances in chondrites and in the North American Shale Composite (NASC) are from Taylor and McLennan, 1985].

Figure 15 depicts relationships between the normalized ratios Tb/Lu, La/Sm and Eu/Eu*. It can be seen that:

- i. as far as the La/Sm ratio is concerned (Fig. 15a, b), samples split into two clusters: the first one, characterized by $La/Sm > 1$, contains all the wallrock (limestone, phosphatic limestone, dolostone) and fluorite type F11a samples; the second (characterized by $La/Sm < 1$), contains all the samples belonging to types F11b, F12 and F13.
- ii. the Tb/Lu ratio remains almost constant for all samples (Fig. 15a).
- iii. Eu/Eu* ratios of the fluorite-bearing samples range from 0.57 to 1.1; 70% of values falling between 0.6 and 0.8. This suggests that the ratio has remained almost constant during the crystallization processes.

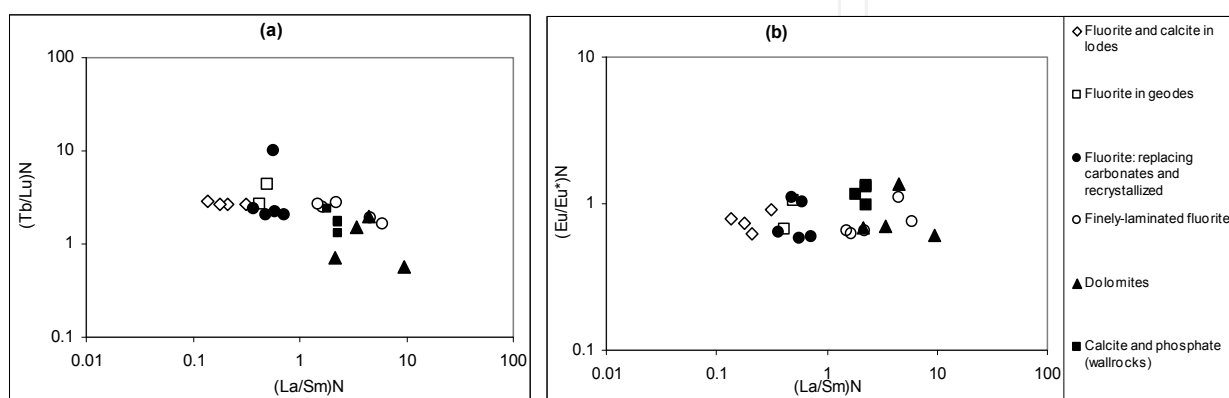


Fig. 15. Relations between chondrite normalized REE ratios of the wallrock minerals and the different petrographic types of fluorite. (a): $(Tb/Lu)_N$ vs. $(La/Sm)_N$; (b): $(Eu/Eu^*)_N$ vs. $(La/Sm)_N$.

8.3 Strontium isotopes

It is well known that strontium (as Sr^{2+}) enters the lattice of gangue minerals such as calcite, dolomite, fluorite and barite. On the other hand, these minerals typically contain negligible concentrations of rubidium. Their $^{87}Sr/^{86}Sr$ ratios thus represent a measure of the isotopic composition of Sr in the mineralizing fluids and do not need to be corrected (Barbieri et al., 1987; Ruiz et al., 1988; Valenza et al., 2000; Sallet et al., 2005). These ratios can therefore be used to identify the reservoirs from which ore fluids have derived their strontium (Kessen et al., 1981).

Strontium isotope analysis has been conducted on six fluorite and two carbonate (dolomite, calcite) samples. The fluorite samples belong to different ore facies: (i) microcrystalline fluorite (L3-21F), associated with finely-laminated karst deposits (type F11a); (ii) dark microcrystalline fluorite (FZ-5N) of the banded ore (type F11a); (iii) white (JS1-6F), and purple (CC3-2)-macrocrystalline fluorites, associated with Carixian phosphatic limestone (type F11b); (iv) megacrystalline fluorite (JS5-F), occurring in a subvertical lode (type F12). The sampled carbonates consist of: (v) white sparry dolomite (DZ-6J) cementing the dolomitic dissolution breccia at the top of the Oust Formation; and (vi) megacrystalline calcite (JS5-C) associated with fluorite JS5-F in the subvertical lode. The samples are described in Table 1. Results (Table 5, Fig. 16) show that, apart from the fluorite sample CC3-2 ($^{87}Sr/^{86}Sr = 0.708613 \pm 12$), which is associated with the Carixian phosphatic

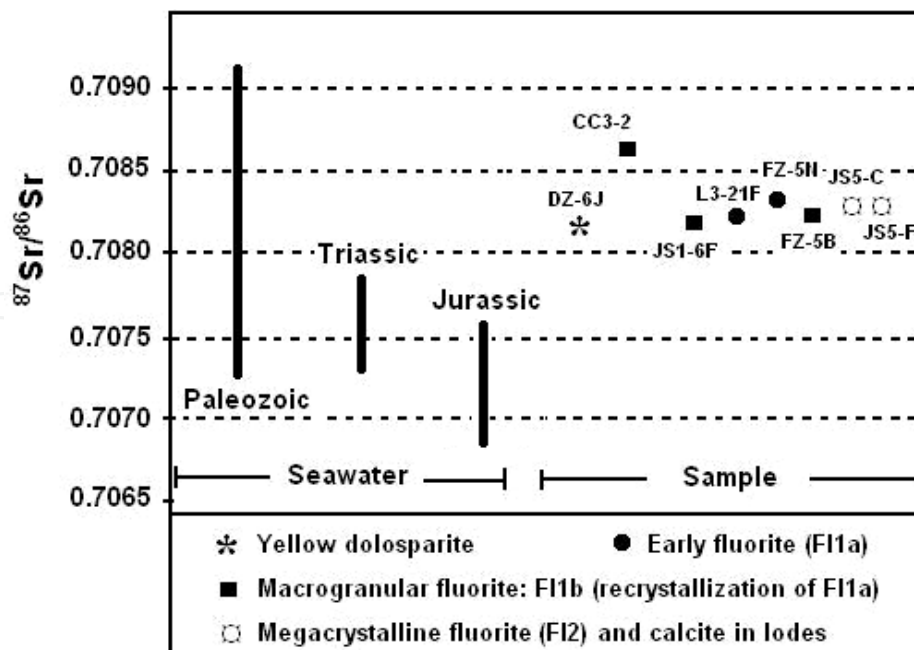


Fig. 16. $^{87}\text{Sr}/^{86}\text{Sr}$ ratios of the wallrocks (DZ-6J), the fluorite ore samples and the associated calcite (JS5-C). Isotopic strontium intervals of the Jurassic and Triassic sea water are from Burke et al. (1982) and Koepnick et al. (1990); those of the Paleozoic are from Burke et al. (1982).

limestone layer, all the Sr isotope ratios fall into a narrow range between 0.708154 ± 8 and 0.708333 ± 8 . The high value of sample CC3-2 could be attributed to enrichment in radiogenic Sr due to the presence of a Rb-bearing phase in the detrital fraction of the karst deposits (e.g., sample L5-15, Table 5). However, these ratios are higher than both Jurassic and Triassic seawater (0.70677 to 0.70778 and 0.70690 to 0.70794, respectively; Burke et al., 1982; Koepnick et al., 1990). Consequently, the mineralizing fluid at Jebel Stah is related to more radiogenic basinal brines derived from even more-deeply buried sedimentary strata.

9. Discussion

The deposition temperature ($135 \pm 20^\circ\text{C}$) of the early fluorite (F11a, F11b) suggests a burial depth of 3500 m to 5000 m in the case of a normal geothermal gradient (25 to $30^\circ\text{C}/\text{km}$). So, as proposed previously for the whole of northern part of Tunisia (Perthuisot et al., 1978; Ben Dhia, 1987a, b), an abnormally regional geothermal gradient prevailed during the deposition of fluorite. The multitude of the depositional phases (generations I and II of fluorite, succeeded by massive quartz) shows that this gradient prevailed over a long period of time. The presence of many geothermal sources in the region (Oust, 58°C ; Zriba, 45°C ; Jedidi, 60°C); (Jellouli, 1973) gives another evidence about the presence of the high regional gradient, and its continuity until today.

The circulation of the highly saline mineralizing fluids was induced by a major post-Jurassic extensional phase. Massive quartz generated subsequently to fluorite from a weakly saline and gaseous CO_2 -rich fluid. The late heating observed during the depositional history at Jebel Stah should be related to the opening of fractures within a such geothermal context. The deposition of fluorite could have resulted from the interference between many

parameters: pressure decrease due to tectonic relaxation during extensional phases; temperature decrease during the ascent of hydrothermal fluids, as well as increase in the dissolved Ca^{2+} activity caused by the dissolving of the carbonate host rocks. The occurrence of the mineralization along the unconformity surface at the top of a carbonated paleorelief which has undergone a strong epigenetic dolomitization, the temperature ($135 \pm 20^\circ\text{C}$) and the salinity (20 ± 1 wt % NaCl eq.) of the fluids which deposited the main body of fluorite, as well as the presence of a minor liquid hydrocarbon phase in late fluorite and massive quartz, allow to compare the fluorite deposit of Jebel Stah to the Mississippi Valley-type group (Roedder, 1984; Anderson and McQueen, 1988; Sangster et al., 1994), especially to those dominated by fluorite in the USA, such as those of Southern Illinois (Grogan and Shrode, 1952; Hall and Friedman, 1963) or Sweetwater-Tennessee (Grogan and Bradburry, 1967; Zimmerman and Kesler, 1981; Vietz and Leach, 1990).

The geochemical results presented in this work are innovative since they deal with a Jurassic mountain district. To our knowledge, only two ore deposits, both located in the domes area of Tunisia, have, until now, been investigated with respect to their REE and Sr-isotope geochemistry. These are the Bougrine Zn-Pb deposit (Sr isotope ratios; Orgeval, 1994) and the Jebel Doghra Sr deposit (REE geochemistry; Souissi et al., 2007). In addition to that, this work provides the first geochemical results relative to the microgranular fluorite associated to the finely laminated karst deposits, and considered as the most early phase of the ore of Jebel Stah (type F11a). Note that, previous studies based on FI microthermometry and geochemistry (Souissi et al., 1997, 1998) have not allowed the characterization of this fluorite type.

The MTE geochemical data allow us to point out that the dolomitization and mineralization processes were accompanied by geochemical exchange between host rocks and fluids. Indeed, the Lower Liassic limestones are not anomalous in MTE, whereas the Carixian phosphatic limestones are highly anomalous with respect to Zn and Cd. The dolomitized horizons are enriched in Mn and Zn in comparison with the wallrock limestones. This suggests that high contents of these elements have been transported in a dissolved state by the dolomitizing fluid. Nevertheless, part of the Zn should have been derived from dissolution of the Carixian phosphates.

The early ore facies (F11a) consisting of the mineralized-finely-laminated karst deposits of the Carixian layer is anomalous in Zn, Cd and Pb, but it is admitted that these elements are contained in the reworked micro-phosphatic debris accumulated in the karsts rather than in the epigenetic fluorite portion of the ore. The recrystallization of the aforementioned fluorite facies and the subsequent remobilization of fluorite in open spaces, (giving rise to F11b, F12 and F13, respectively), took place in the presence of an evolved fluid which was depleted in Mn and enriched in Co. Most of the Mn load was taken up by carbonates during the dolomitizing process, while Co has been concentrated in the residual fraction of the fluid.

The REE geochemistry results allowed differences between the wallrock limestones and the fluorite-bearing samples to be identified. Indeed, the $\sum\text{REE}$ values are low in the aforementioned limestones (0.35 to 2 ppm), in accordance with the rather low REE concentrations (<10 ppm) reported for sedimentary carbonate rocks (Taylor and McLennan, 1985; Chetty and Frimmel, 2000). Although higher values are recorded in the phosphatic limestones (≈ 24 ppm), $\sum\text{REE}$ values are, however, significantly below their analogues in

Eocene formations of the phosphate basins of Central and Southern Tunisia (100 to 2,140 ppm and 50 to 1,950 ppm, respectively; Sassi, 1999).

Among the fluorite-bearing samples, the results have shown that the highest Σ REE values (7.25 to 65.4 ppm), are recorded for early F11a fluorite associated with finely-laminated karst deposits. These values are due to the presence of remnant phosphate, as well as to clay minerals in the matrix. Clay minerals typically have much higher Σ REE compared to the other fractions in sediments (Bellanca et al., 1981; McLennan, 1989). The recrystallization of F11a facies gives rise to the white-to-purple macrogranular fluorites of type F11b, characterized by Σ REE values (0.8 to 1.6 ppm) which are too low with respect to the inferred parent material. Megacrystalline fluorites F12 and F13, occurring within open spaces (lodes and cavities, respectively), bear the lowest Σ REE values. The decrease in REE contents in the later fluorites indicates that, during crystallization, the ore fluid becomes depleted in these elements (Schönenberger et al., 2008). However, the megacrystalline calcite in the vertical lodes is characterized by Σ REE values (5 to 18.35 ppm), higher than those in the coeval fluorite. Such values show that in open spaces, REE are fractionated between the two minerals, permeating more easily into the carbonate phase.

Σ REE values of the fluorites under consideration are, on the whole, low in comparison with fluorites from other hydrothermal deposits, such as those of the d'El Hammam district, Morocco (Jebrak et al., 1984), the main fluorite occurrences in Brazil (Dardenne and Touray, 1988; Ronchi et al., 1993), the North Pennines of England (Shepherd et al., 1982) or the Marche occidentale, France (Grappin et al., 1979). They are, however, similar to those recorded for fluorites from the Asturian Province, Spain (Ferrand et al., 1978), the Tarn in France (Hubert et al., 1982) and the Eastern-Alpine area in Germany (Schneider et al., 1975).

The chondrite-normalized REE patterns allow differences between the wallrocks unaltered by hydrothermal circulation (limestone, phosphatic limestone) and the dolostones and different ore facies to be identified. Calcite and apatite of the wallrock layers have acquired their REE imprint during diagenesis of Lower-Middle Liassic sediments in equilibrium with seawater trapped in the interstitial porosity. The REE patterns of the dolomites plot within the field of their hydrothermal homologues (Henderson, 1984). The hydrothermal origin of the epigenetic dolomites was demonstrated earlier by Souissi et al. (1998), on the basis of petrographic analysis and fluid inclusion microthermometry. The latter authors pointed out that the dolomitization and deposition of the exploitable ore (fluorites F11a, F11b and F12) took place under the same conditions. Therefore, and by taking into account that both the epigenetic dolomites and the microgranular-early fluorite (F11a) are characterized by similar REE patterns, reproducing that of the NASC (Taylor and McLennan, 1985), it is believed that this geochemical imprint was inherited from a fluid that had remained in equilibrium with deep shales. Such a statement leads to the conclusion that all the samples of this group may be considered as coeval (Dardenne and Touray, 1988). The preferential concentration of LREE [$(\text{Tb}/\text{La})_N < 1$] indicates that fluorite F11a belongs to the early stage of crystallization (Ekambaram et al., 1986; Subias and Fernandez-Nieto, 1993; Schönenberger et al., 2008). LREE depletion, for both the macrocrystalline fluorites (F11b) resulting from recrystallization of type F11a, or the megacrystalline fluorites F12 and F13, occurring in open spaces, provide evidence for REE fractionation during the later stages of mineralization (Ekambaram et al., 1986) in a closed system. Similar REE patterns are reported by Subias and Fernandez-Nieto (1993) for late hydrothermal fluorites from the Valle de Tena, Spanish Central Pyrenees, hosted in

Paleozoic pelitic, psammitic and carbonatic rocks. According to Richardson and Holland (1979) and Tropper and Manning (2007), the solubility of fluorite strongly increases in chloride-rich solutions (≈ 20 wt % NaCl equivalent at Jebel Stah). Strong et al. (1984) state, however, that REE are dominantly present as fluoro-complexes in such solutions. The observed LREE depletion and relative HREE enrichment are justified by a dissolution-reprecipitation process with a decrease of fluorine activity in the fluids. This process causes the changing of REE from difluoro- to monofluoro-complexes, and thus, a decreasing ability of the hydrothermal solutions to transport LREE with respect to HREE (higher stability of HREE monofluoro-complexes; Henderson, 1984; Strong et al., 1984; Ronchi et al., 1993).

The weak negative Ce and Eu anomalies seen in all REE patterns for fluorites and other fluorite-bearing samples (dolostones and finely laminated karst deposits) are assumed to record the signature of the hydrothermal fluoride-bearing solution. Regarding the Ce anomaly, Bellanca et al. (1981) defend the hypothesis that this anomaly occurs when fluorite crystallizes from solutions which are derived from sediments with high oxygen fugacities. In such environments, Ce becomes oxidized prior to mobilization, resulting in a lower migration coefficient for Ce^{4+} than would be the case for the trivalent ions of the other REE. The REE patterns of all fluorite-bearing samples and the associated calcites are slightly depleted in Eu. Such a depletion characterizes all post-Archean sedimentary rocks (Taylor and McLennan, 1985; McLennan, 1989).

In addition, all fluorites - regardless to their petrographic types - are characterized by Sm/Yb ratios of 1.02 to 5.5, close to values commonly measured in shales (about 2.0). This is consistent with REE derived from siliciclastic sources, or even from the dissolution of LREE-enriched evaporates (Cai et al., 2008).

Taking the ratios La/Sm, Tb/Lu and Eu/Eu* into consideration, information has been gathered about the fluid properties, along with REE behaviour during all the epigenetic processes (dolomitization, deposition of early-stage fluorite and its further recrystallization or remobilization to be redeposited in open spaces). From the La/Sm ratios, it has been deduced that the dolomites and early fluorite (F11a) have been generated from a fluid which is geochemically different from the one that gave rise to the late fluorites (F11b, F12 and F13). Being depleted in LREE, the second fluid is generated from the residual fraction of the above-mentioned one. Therefore, the uniformity of the Tb/Lu ratios, allowed us to deduce that, unlike the LREE, the HREE did not undergo fractionation during the crystallization process. On the other hand, it is well established that the oxidation state of Eu incorporated in hydrothermal minerals provides an additional tool to constrain the chemistry of ancient fluids and the mechanisms responsible for mineral precipitation (Brugger et al., 2008). In this respect, the uniformity of the Eu/Eu* ratios provides evidence that the fluorites contain Eu predominantly as Eu^{3+} and might have crystallized from relatively oxidized fluids that bear very small inherited Eu anomalies (Ghaderi et al., 1999; Schönerberger et al., 2008). Therefore, and according to Sverjensky (1984) and Bau and Möller (1992), temperature is the most important parameter controlling the Eu^{3+}/Eu^{2+} redox potential in hydrothermal environments. At temperatures exceeding 250 °C, Eu^{2+} dominates over Eu^{3+} and may substitute for Ca^{2+} preferentially over trivalent REE, leading to positive Eu anomalies in mineral precipitates. The lack of any positive Eu_{CN} anomaly, for either the epigenetic dolomites or the fluorites considered in this study thus indicates that the fluid from which they were precipitated never reached such high temperatures (Schönerberger et al., 2008; Uysal et al., 2008).

The determination of the $^{87}\text{Sr}/^{86}\text{Sr}$ ratios for the epigenetic carbonates (dolomite, calcite) and fluorite showed a uniformity of this ratio throughout the deposit, providing evidence for isotopic homogeneity (Ayuso et al., 2004) and, consequently, the identity of the source of the mineralizing fluid. As deduced from the aforementioned petrographic analysis, fluid inclusion microthermometry and REE geochemistry, these observations strongly support the idea that dolomitization and mineralization were produced by the same hydrothermal system (Savard et al., 2000). Since they are higher than those of both the Jurassic or the Triassic seawater, these ratios might, however, be interpreted in terms of basinal brines, trapped within the Paleozoic sedimentary column, which should be characterized by even higher Sr isotopic ratios (0.7067 to 0.7091; Burke et al., 1982; Fig. 16). The measured ratios fall within the range of all Pennsylvanian, Late Devonian, Lower Silurian and Middle Ordovician $^{87}\text{Sr}/^{86}\text{Sr}$ intervals. In Tunisia, apart from the marine-Permian outcrop of Jebel Tebaga, the Paleozoic series is known in Southern Tunisia only at subsurface thanks to oil-field drilling programs (Memmi et al., 1986). The sedimentary series (sandstones, siltstones, shale, carbonates) are related to the well-oxygenated-shallow environments of the continental shelf (Chauvel and Massa, 1981). They are represented by megasequences (>10 km-thick), rich in detrital fraction and separated by major discontinuities (Buroillet and Busson, 1983). The Precambrian basement is made of phyllites along with granodiorites and granites cut by acid and basic volcanic rocks (Bajanik, 1972). The present authors support the idea that the radiogenic Sr measured in the fluorite ore deposit of Jebel Stah could have been sourced in the connate waters trapped in the Paleozoic sedimentary column. Thus, the mineralizing fluids relate to deep thermally-driven basinal fluid circulations (Souissi et al., 1997, 1998, 2010). In another respect, the same authors have pointed out that deposition of the ore at Jebel Stah, hosted in the Lower-Middle Liassic layers, took place at $135 \pm 20^\circ\text{C}$, from a fluid derived from a reservoir where temperature was $275 \pm 25^\circ\text{C}$ on average. The difference in temperature is in the order of 140°C . Assuming a mean geothermal gradient of $50^\circ\text{C}/\text{km}$, according to the estimations of Perthuisot (1978), Perthuisot et al. (1978) and Ben Dhia (1987a, b), the reservoir should be 2.5 to 3 km below the deposition level. This interval should include the Lower Liassic (≤ 700 m), the Triassic (> 1000 m; Bonnefous, 1972) and the upper part of the Paleozoic series.

Remobilization of deep-seated primary deposits, hosted in the Paleozoic sequence, seems to be a very plausible hypothesis, especially as Zn-Pb-Ba veins are hosted in the "Upper Dolostones" of Late Permian age at Jebel Tebaga in Southern Tunisia (Sainfeld, 1952). The same hypothesis is also strongly supported by the presence of several intra-Paleozoic fluorite ores hosted in a sedimentary series to which magmatic events may be associated and that are documented all around the Mediterranean basin. These include: (i) in France, the Tarn department (Couturier, 1980; Béziat et al., 1982; Deloule, 1982), the Pyrénées-Atlantiques (Martin, 1979; Thibieroz, 1982) and the Cordesse (Marchand et al., 1976); (ii) in Spain, the Asturian province (Garcia-Iglesias and Loredó, 1982; Ferrand et al., 1978) and the Valle De Tena in the Huesca Province (Subias and Fernandez-Nieto (1993); (iii) In Italy, the Sarrabus area of Sardinia (Harvey et al., 1984).

The hypothesis of a deeply-seated origin for the metal-bearing fluids in northern Tunisia is now largely accepted (Perthuisot et Saliot, 1979; Rouvier et al., 1985; Orgeval, 1994; Sheppard et al., 1996; Souissi et al., 1997, 1998, 2007, 2010; Decrée et al., 2008; Jemmali et al., 2011). Fluid circulation is triggered in response to hydraulic fracturing in high geothermal gradient settings, especially along the major structural trends (Ben Dhia, 1987a, b). Such

geothermal-gradients prevailed for a long time and are evidenced either by SHMS-Sedex ore deposits in the Bougrine area within the Dome Zone related to the Cenomano-Turonian period (Orgeval, 1994), to the Upper Miocene in the area of Sidi Driss-Dhouahria farther North, within the Nappe Zone (Decrée et al., 2008), or to Miocene magmatic activity (rhyodacites, granodiorites), with which Fe-, Mn-, Pb-, Zn-, Cu-, Ag- and F-bearing mineralization is associated in the latter zone (Bellon, 1976; Laridhi-Ouazaa, 1994).

10. Conclusions

The F-(Ba, Pb, Zn) deposits of northern Tunisia have been previously considered as the result of continental alteration and sedimentation (Florida, 1973; Fuchs, 1973; Thibieroz, 1974 and 1976; Touhami, 1979). This study gives evidence that the fluorite deposit of Jebel Stah resulted from the replacement of carbonate rocks after they underwent an epigenetic dolomitization along the intra-Liassic unconformity, located at the top of a paleorelief. The economic ore (fluorite I: Fl1a, Fl1b, Fl2) as well as the dolomitic DCRs structures resulted from highly saline (20 ± 1 wt % NaCl eq.) Na-Ca-Cl hydrothermal (135 ± 20 °C) brines. Later on, a less saline (10 ± 1 wt % NaCl eq.) and warmer (185 ± 20 °C) fluids deposited fluorite within geodes (fluorite II). In the last stage, silica and minor fluorite deposited within fractures owing to the circulation of a low salinity (5.5 ± 1 wt % NaCl eq.) but yet warmer (225 ± 20 °C) and CO₂-rich fluid. These fluids probably arose from the reservoir where the temperature was on average 275 ± 25 °C. This study confirmed the existence of a high regional geothermal gradient, which prevailed over a long period of time extending probably since the Upper Miocene until today. So, the late heating observed during the depositional history of fluorite and quartz at Jebel Stah, should be related to the opening of fractures during extensional phases within a such geothermal context. Deposition of the workable fluorite ore has at Jebel Stah resulted from the decrease in temperature and the increase of the calcium activity due to dissolution of carbonate rocks. Taking the geological framework, the epigenetic character of the ore deposit, the mineralogical association and the temperature and composition of the fluids into consideration, the fluorite ore deposit of Jebel Stah is considered to represent a fluorite-dominant MVT-type deposit.

The MTE, REE and Sr isotope geochemistry gives new arguments to support the genetic model for fluorite ore at Jebel Stah. Both petrography and REE geochemistry show a close spatial and temporal association between the epigenetic dolomitization that affected the Lower-Middle Liassic host carbonates and the subsequent fluorite ore deposition. This association, along with the REE and Sr isotope geochemistry of epigenetic carbonates (dolomite, calcite) and fluorite, shows that dolomitization and mineralization were produced by the same hydrothermal system and indicate that at least part of the fluoride has been transported in solution as MgF⁺ complexes by an oxidized fluid derived from a sedimentary basin. The source of this fluoride is suggested to be the geological sequence underlying the Lower-Middle Liassic horizons that host the fluorite ore. These results are in accordance with those of Souissi et al. (1997, 1998) who supposed, on the basis of microthermometric and geochemical analysis of fluid inclusions, that the mineralizing fluids giving rise to F-(Ba,Pb,Zn) deposits in the Zaghouan district, may be assimilated to basinal brines (connate waters) released by hydraulic fracturing during a major post-Jurassic and most probably an Upper Miocene extensional phase. Recently, a similar age is accepted for several mineralizations occurring in northern Tunisia (Decrée et al., 2008; Souissi et al., 2010;

Jemmali et al., 2011). The Triassic units are the least probable source for the fluoride, especially if one takes into consideration the results of the Sr isotope study, as well as the scarcity of this element in the remaining geological zones of northern Tunisia (Trough zone, Dome area, Nappe zone). The Paleozoic series is the preferred source of the mineralizing fluids and remobilization of primary fluorite ores, hosted in this series, seems to be a plausible hypothesis. If true, the large distribution of the deposits in space and time, throughout the district of Zaghouan, indicates that the buried stocks should be of paramount importance.

It is suggested that the Paleozoic series, cropping out nowhere in the Jurassic mountains area of North-Eastern Tunisia, may potentially bear significant primary F-(Pb, Zn, Ba, Sr) reserves. Taking into account both the geological and geothermal settings, such deposits should lay between the reservoir of the fluids (Upper part of the Paleozoic series) and the Paleozoic-Triassic contact (1500 to 2000 m beneath the Lower-Middle Liassic contact at the locality of Jebel Stah and in the neighbouring area of Jebel Kohol).

11. References

- Ames L. (1955). Chemical analysis of the fluid inclusions in a group of New Mexico minerals. *Econ. Geol.*, 53, pp. 473-480.
- Anderson G.M & McQueen R.W. (1988). Mississippi Valley-type lead-zinc deposits. In: *Ore deposit models*, Roberts R.G. and Seahan P.A., pp. (79-90). Geoscience, Geological Association of Canada publications, Ottawa, Reprint 3.
- Ayuso R.A., Kelley, K.D., Leach, D.L. & Young, L.E. (2004). Origin of the Red Dog Zn-Pb-Ag deposits, Brooks Range, Alaska: Evidence from regional Pb and Sr isotope sources. *Economic Geology*, 99, pp. 1533-1553.
- Badgasarian G.P., Bajanik S. & Vass D. (1972). Age radiométrique du volcanisme néogène du Nord de la Tunisie. *Notes Serv. Géol. Tunisie*, 40, pp. 79-85.
- Bajanik S. (1972). Précambrien en Tunisie (Plateforme saharienne). *Notes du Service Géologique de Tunisie*, 40, pp. 5-17.
- Barbieri M., Bellanca A., Neri R. & Tolomeo L. (1987). Use of strontium isotopes to determine the sources of hydrothermal fluorite and barite from Northwestern Sicily (Italy). *Chemical Geology*, 66, pp. 273-278.
- Bau M. & Möller P. (1992). Rare-earth element fractionation in metamorphogenic hydrothermal calcite, magnesite and siderite. *Mineralogy and Petrology*, 45, pp. 231-246.
- Bau M., Romer R.L., Lüders V., Dulski P. (2003). Tracing element sources of hydrothermal mineral deposits: REE and Y distribution and Sr-Nd-Pb isotopes in fluorite from MVT deposits in the Pennine Orefield, England. *Mineralium Deposita*, 38, pp. 992-1008.
- Beales F.W. (1971). Cementation by white sparry dolomite. In: *Carbonate cements*, Bricker O.P., pp. 330-338, Johns Hopkins Univ Press, Baltimore.
- Beales F.W. & Hardy J.L. (1980). Criteria for the recognition of diverse dolomite types with an emphasis on studies on host rock for Mississippi Valley-type ore deposits. In: *Concepts and models of dolomitization*, Zenger D.J., Dunham J.B. & Etlington R.L., pp. 197-213, SEPM Spec Nr 28.

- Bellanca A., Di Salvo P., Möller P., Neri R. & Schley F. (1981). Rare earth and minor element distribution and petrographic features of fluorites and associated Mesozoic limestones of Northwestern Sicily. *Chemical Geology*, 32, 255-269.
- Bellon H. (1976). Séries magmatiques néogènes et quaternaires du pourtour de la Méditerranée occidentale comparées dans leur cadre géochronologique. Implications géodynamiques. *Thèse Doct. ès Sciences*, Université d'Orsay.
- Ben Dhia H. (1987a). The geothermal gradient map of central Tunisia: Comparison with structural, gravimetric and petroleum data. *Tectonophysics*, 142, pp. 99-109.
- Ben Dhia H. (1987b). La carte du gradient géothermique de Tunisie- Etablissement à partir de données de températures particulières. *Bulletin Centre Recherche Exploration Production Elf Aquitaine*, II (2), pp. 221-231.
- Beziat P., Bles J.L., Fortuné J.P. & Lhegu J. (1982). Les filons à fluorine de l'Albigeois; présentation générale, guide de prospection. *Bulletin du BRGM*, section II (4), pp. 417-426.
- Bodnar R.J. & Bethke P.R. (1984). Systematics of stretching of fluid inclusions, I: fluorite and sphalerite at 1 atmosphere confining pressure. *Economic Geology*, 79, pp. 141-146.
- Bouaziz, S., Barrier, E., Soussi, M., Turki, M. & Zouari H. (2002). Tectonic evolution of the northern African margin in Tunisia from paleostress data and sedimentary record. *Tectonophysics*, 357, pp. 227-253.
- Bouhlef S. (1982). Distribution du baryum et du strontium dans la province fluorée tunisienne; application aux gîtes de Hammam Zriba-Jebel Guebli. *Thèse 3ème Cycle*, Université Toulouse.
- Bouhlef S., Fortuné J.P., Guilhaumou N. & Touray J.C. (1988). Les minéralisations stratiformes à F-Ba de Hammam Zriba-Jebel Guebli (Tunisie nord-orientale): l'apport des études d'inclusions fluides à la modélisation génétique. *Mineralium Deposita*, 23, pp. 166-173.
- Bonnefous J. (1972). Contribution à l'étude stratigraphique et micropaléontologique du Jurassique de Tunisie. *Thèse doctorat ès Sciences Naturelles*, Université de Paris VI.
- Brugger J., Etschmann B., Pownceby M., Liu W., Grundler P. & Brewe D. (2008). Oxidation state of europium in scheelite: Tracking fluid-rock interaction in gold deposits. *Chemical Geology*, 257, pp. 26-33.
- Burke W.H., Denison R.E., Hetherington E.A., Koepnick R.B., Nelson H.F. & Otto J.B. (1982). Variation of sea water $^{87}\text{Sr}/^{86}\text{Sr}$ throughout Phanerozoic time. *Geology*, 10, pp. 516-519.
- Burollet P.F. & Busson G. (1983). Plateformes et bassins. Danger d'un actualisme exagéré. *Notes et Mémoires de la Compagnie Française des Pétroles*, Paris 18, pp. 9-16.
- Cai C., Li K., Li. H. & Zhang B. (2008). Evidence for cross formational hot brine flow from integrated $^{87}\text{Sr}/^{86}\text{Sr}$, REE and fluid inclusions of the Ordovician veins in Central Tarim, China. *Applied Geochemistry*, 23, pp. 2226-2235.
- Castany G. (1954). Les grands traits structuraux de la Tunisie. *Bull. Soc. Géol. France*, section IV (6), pp. 151-173.
- Chauvel J.C. & Massa D. (1981). Paléozoïque de Libye occidentale. Constantes géologiques et pétrographiques. Signification des niveaux ferrugineux oolithiques. *Notes et Mémoires de la Compagnie Française des Pétroles*, Paris, 16, pp. 25-66.
- Chetty D. & Frimmel H.E. (2000). The role of evaporates in the genesis of base metal sulfide mineralisation in the northern platform of the Pan-African Damara belt, Namibia:

- geochemical and fluid inclusion evidence from carbonate wall rock alteration. *Mineralium Deposita*, 35, pp. 364-376.
- Choquette RW (1971) Late ferroan dolomite cement, Mississippian carbonates, Illinois Basin USA. In: *Carbonate cements*, Briker O.P., pp. (339-346), Johns Hopkins Univ Press, Baltimore.
- Couturier P. (1980). Contribution à l'étude géologique et gîtologique du district à fluorine de l'Albigeois cristallin. *Thèse de 3^{ème} cycle*, Université de Toulouse.
- Crawford M.L. (1981). Fluid inclusions in metamorphic rocks. Low and medium grade. In: *Short course on fluid inclusions: application to ore petrology*, Hollister L.S. & Crawford M.L., pp. (157-181), Mineralogical Association of Canada, Calgary.
- Dardenne M.A. & Touray J.C. (1988). La fluorine du Brésil. Gisements filoniens traditionnels et nouveaux types de minéralisations. *Chronique de la Recherche Minière*, 490, pp. 5-46.
- Decrée S., Marignac C., De Putter T., Deloule E., Liegeois J.P. & Demaiffe D. (2008). Pb-Zn mineralisation in a Miocene regional extensional context: the case of the Sidi Driss and the Dhouahria ore deposits (Nefza mining district, Northern Tunisia). *Ore Geology Reviews*, 34, pp. 285-303.
- Deloule E. (1982). The genesis of fluorite hydrothermal deposits at Montroc and Le Burc, The Tarn as deduced from fluid inclusion analysis. *Economic Geology*, 77, pp. 1867-1874.
- Ekambaram V., Brookins D.G., Rosenberg P.E. & Emanuel K.M. (1986). Rare earth element geochemistry of fluorite-carbonate deposits in Western Montana, U.S.A. *Chemical Geology*, 54, pp. 319-331.
- Ellis A.J. (1970). Quantitative interpretation of chemical characteristics of hydrothermal systems. *Geothermics*, Spec Iss 2, pp. 516-528.
- Ferrand A., Grappin C., Garcia-Iglesias J. & Touray J.C. (1978). Nouvelles données sur le gîte de fluorine de Villabona (Asturies-Espagne) et ses conditions de genèse. *Bulletin du BRGM*, section II (4), pp. 357-369.
- Florida S. (1973). La province fluorée tunisienne. Aperçu géologique et métallogénique. In: *Livre jubilaire M. Solignac*, Ann. Mines Géol. Tunis, 26, pp. 459-477.
- Folk R.L. and Assereto R. (1974). Giant aragonite rays and baroque white dolomite in tepee-fillings. Triassic of Lombardy, Italy (abst.). AAPG, Abst., Ann. Meet., San Antonio, pp. 34-35.
- Fontboté L. (1981). Stratabound Zn-Pb-F-Ba deposits in carbonate rocks: new aspects of paleogeographic location, facies factors and diagenetic evolution (with a comparison of occurrences from the Triassic of Southern Spain, the Triassic-Liassic of Central Peru and other localities). *PhD thesis*, Heidelberg University.
- Fontboté L. (1993). Self-organization fabrics in carbonate-hosted ore deposits: the example of diagenetic crystallization rhythmites (DCRs). In: *Current Research in Geology applied to ore deposits*, Fenoll Hach-Ali P., Torres-Ruiz J., Gervilla F., pp. 11-14, Proceedings of the second biennial SGA Meeting, 84-338-1772-8, Granada,
- Fontboté L. & Amstutz G.C. (1983). Facies and sequence analysis of diagenetic crystallization rhythmites in stratabound Pb-Zn-(Ba-F) deposits in the Triassic of Central and Southern Europe. In: *Mineral deposits of the Alps and of the Alpine Epoch in Europe*, Schneider H.G., pp. 347-358, Springer, Berlin-Heidelberg-New York.

- Fontboté L. & Gorawski H. (1990). Genesis of the Mississippi Valley-type Zn-Pb deposit of San Vicente Central Peru: geological and isotopic (Sr, O, C, S) evidences. *Economic Geology*, 85, pp. 1402-1437.
- Fournier R.O. & Trusdell A.M. (1973). An empirical Na-K-Ca geothermometer for natural waters. *Geochim Cosmochim Acta*, 37, pp. 1255-1275.
- Fuchs Y. (1973). Sur les relations entre émergence et concentrations métallifères, quelques exemples tunisiens. In : *Livre jubilaire M. Solignac*, Ann. Min. Géol. Tunis, 26, pp. 480-509.
- Garcia-Iglesias J. & Loredó-Perez J. (1982). Conditions physico-chimiques de formation des minéralisations à fluorine de la province des Asturias (Espagne): corrélation et synthèse. *Bulletin du BRGM*, section II (4), pp. 353-357.
- Ghaderi M., Palin J.M., Campbell I.H. & Sylvester P.J. (1999). Rare earth element systematics in scheelite from hydrothermal gold deposits in the Kalgoorlie-Norseman Region, Western Australia. *Economic Geology*, 94, pp. 423-438.
- Grappin C., Treuil M., Yaman S. & Touray J.C. (1979). Le spectre des terres rares de la fluorine en tant que marqueur des propriétés du milieu de dépôt et des interactions entre solutions minéralisantes et roches sources. Exemple pris dans le district de la Marche occidentale (France). *Mineralium Deposita*, 14, pp. 297-309.
- Gregg J.M. & Sibley D.F. (1984). Epigenetic dolomitization and the origin of xenotopic dolomite texture. *J. Sediment. Petrol.*, 54, pp. 908-931.
- Grogan R.M. & Bradburry J.C. (1967). Origin of the stratiform fluorite deposits of Southern Illinois. In: J.S. Brown Ed., Genesis of stratiform lead-zinc-barite-fluorite deposits (Mississippi Valley-type deposits). *Economic Geology*, Monogr. 3, pp. 40-51.
- Grogan R.M. & Shrode R.S. (1952). Formation temperatures of Southern Illinois bedded fluorite as determined from fluid inclusions. *Amer. Mineral.*, 37, pp. 555-566.
- Hall W.E. & Friedman I. (1963) Composition of fluid inclusions, Cave-in-Rock fluorite district, Illinois and Upper Mississippi Valley zinc-lead district. *Economic Geology*, 58, pp. 886-911.
- Harvey E.B., De Vivo B. & Valera R. (1984). Fluid inclusion study of some Surrabus fluorite deposits, Sardinia, Italy. *Economic Geology*, 79, pp. 409-414.
- Henderson P. (1984). Rare earth elements geochemistry. In: *Developments in Geochemistry*, Vol. 2, Henderson P., Elsevier, Amsterdam.
- Hubert P., Joron J.L., Touray J.C. & Treuil M. (1982). Le spectre des lanthanides de la fluorite, indicateur possible de l'origine et de l'histoire des solutions hydrothermales. Application au district du Tarn (France). *Bulletin du BRGM*, section II (4), pp. 365-369.
- Jacquin J.P. (1970). Contribution à l'étude géologique et minière de la Sierra de Gador (Almeria, Espagne), Tome II, Géologie Minière. *Thèse 3^{ème} cycle*, Université de Nantes.
- Jebrak M., Debbah B. & Touray J.C. (1984). Saumures associées aux fluorines filoniennes du Maroc central dans le district d'El Hammam. *Bulletin de Minéralogie*, 107, pp. 233-240.
- Jellouli A. (1973). Géochimie de quelques sources thermo-minérales de Tunisie. In : *Livre jubilaire M. Solignac*, Ann. Min. Géol. Tunis, 26, pp. 571-579.

- Jemmali N., Souissi F., Villa I.M. & Vennemann T.W. (2011). Ore genesis of Pb–Zn deposits in the Nappe zone of Northern Tunisia: Constraints from Pb–S–C–O isotopic systems. *Ore Geology Reviews*, 40, pp. 41–53.
- Kessen K.M., Woodruff M.S. & Grant N.K. (1981). Gangue mineral $^{87}\text{Sr}/^{86}\text{Sr}$ ratios and the origin of Mississippi Valley-type Mineralization. *Economic Geology*, 76, pp. 913–920.
- Koepnick R.B., Denison R.E., Burke W.H., Hetherington E.A. & Dahl D.A. (1990). Construction of the Triassic and Jurassic portion of the Phanerozoic curve of sea water $^{87}\text{Sr}/^{86}\text{Sr}$. *Chemical Geology (Isotope Geoscience Section)*, 80, pp. 327–349.
- Laridhi-Ouazaa N. (1994). Etude minéralogique et géochimique des épisodes magmatiques mésozoïques et miocènes de la Tunisie. *Thèse Doctorat ès Sciences*, Université de Tunis.
- Marchand L., Joseph D., Touray J.C. & Treuil M. (1976). Critères d'analyse géochimique des gisements de fluorine bases sur l'étude de la distribution des lanthanides. Application au gîte du Maine (71 – Cordesse, France). *Mineralium Deposita*, 11, pp. 357–379.
- Martin F. (1979). Les gisements de fluorine post-hercyniens (karstiques et filoniens) dans le Paléozoïque de la région du Pourtalet (Pyrénées atlantiques – Province de Huesca). *Thèse 3ème cycle*, Université de Paris VI.
- Martini J.E.J. (1976). The fluorite deposits in the dolomite series of the Marico District, Transvaal, South Africa. *Economic Geology*, 71, pp. 625–635.
- Mason B. (1966). *Principles of Geochemistry* (3rd edition). John Wiley and Sons, ISBN 0-471-57526-7, New York.
- McLennan S.M. (1989). Rare earth elements in sedimentary rocks: influence of provenance and sedimentary processes. In: *Geochemistry and mineralogy of rare earth elements*, Ribbe P., pp. (169–200), *Reviews in Mineralogy 21: Geochemistry and mineralogy of rare earth elements*, ISBN 0-939950-25-1, Chelsea-Michigan.
- Memmi L., Burollet P.F. & Viterbo I. (1986). Lexique stratigraphique de la Tunisie. Première partie : Précambrien et Paléozoïque. *Notes du Service Géologique de Tunisie*, 53, pp. 1–66.
- Möller P., Morteani G. & Dulski P. (1984). The origin of calcites from Pb–Zn veins in the Hartz mountains, Federal Republic of Germany. *Chemical Geology*, 45, pp. 91–112.
- Office National des Mines (ONM) (1968). Projet des travaux géologiques de recherche pour le gisement de Djilet Staa Tunisie. Unpublished internal report.
- Office National des Mines (ONM) (1990). Zone fluorée de Zaghouan. Projet de réouverture des mines de Mecella, Jebilet el Kohol, Sidi Taya et Stah. Unpublished internal report.
- Ohle E.L. (1985). Breccias in Mississippi Valley-type deposits. *Economic Geology*, 80, pp. 1736–1752.
- Orgeval J.J., 1994. Peridiapiric metal concentration: example of the Bougrine deposit (Tunisian Atlas). In: *Sediment-hosted Zn-Pb ores*. Society for Geology Applied to Mineral Deposits, Fontboté & Boni, pp. 354–389, Special Publication No 10, , Soc. Geol. Applied to Mineral Deposits, Sediment-Hosted Zn-Pb Ores, Springer, Verlag Berlin Heidelberg.
- Perthuisot, V., 1978. Dynamique et pétrogenèse des extrusions triasiques en Tunisie septentrionale. *Thèse doctorat ès Sciences*, Ecole normale supérieure de Paris.

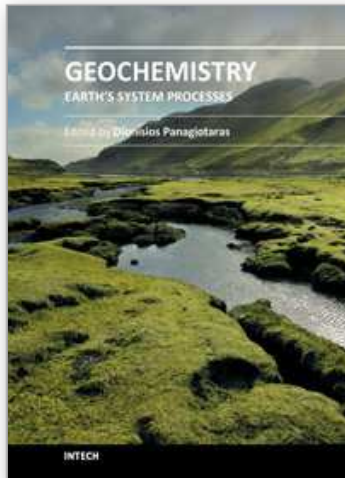
- Perthuisot V., Guilhaumou N. & Touray J.C. (1978). Les inclusions fluides hypersalines et gazeuses de quartz et de dolomites du Trias évaporitique nord-tunisien. Essai d'interprétation géodynamique. *Bulletin de la Société géologique de France*, XX, 2, pp. 145-155.
- Perthuisot V. & Saliot P. (1979). Néoformations silicatées dans le Trias des diapirs tunisiens. Rôle des solutions hydrothermales. *Sciences de la Terre*, XXIII, 2, pp. 75-83.
- Potter R.W. II & Calif M.P. (1977). Pressure corrections for fluid inclusion homogenization temperatures based on the volumetric properties of the system NaCl-H₂O. *J Res US Geol Surv*, 5, pp. 603-607.
- Poty B., Leroy J. & Jachimowicz L. (1976). Un nouvel appareil pour la mesure des températures sous le microscope: l'installation de microthermométrie chaixmeca. *Bull Soc Fr Mineral Cristallogr*, 99, pp. 182-186.
- Potts, P.J., Thompson M., Kane J.S., Webb P.C. and Carignan J. (2000). GeoPT6 - An international proficiency test for analytical geochemistry laboratories - Report on round 6 (OU-3: Nanhoron microgranite) and 6A (CAL-S: CRPG limestone). Unpublished Report, (Report.pdf).
- Prévôt L., Lucas J., Nathan Y. & Shiloni Y. (1979). Répartition des éléments traces dans les phosphorites marines. In: *Origin and distribution of the elements. Second symposium, Physics and chemistry of the Earth volume 11.*, Ahrens, pp. 293-304, ISBN 0-08-022947-6, Oxford.
- Radke B.M. & Mathis M.L. (1980). On the formation and occurrence of Saddle dolomite. *J. Sediment Petrol*, 50, pp. 1149-1168.
- Rakus M. & Biely A. (1970). Stratigraphie du Lias dans la dorsale tunisienne. *Notes du Service Géologique*, 32, pp. 46-63.
- Richardson C.K. & Holland H.D. (1979). The solubility of fluorite in hydrothermal solutions, an experimental study. *Geochimica et Cosmochimica Acta*, 43, pp. 1313-1325.
- Richert J.P. (1971). Mise en évidence de quatre phases tectoniques successives en Tunisie. *Notes du Service Géologique de Tunisie*, 34, pp. 115-125.
- Roedder E. (1963). Studies of fluid inclusions, II: freezing data and their interpretation. *Econ. Geol.*, 58, pp. 167-211.
- Roedder E. (1967). Environment of deposition of stratiform (Mississippi Valley-Type) ore deposits, from studies of fluid inclusions. In: *Genesis of stratiform lead-zinc-barite-fluorite (Mississippi Valley-type deposits)*, pp. 349-362, Econ. Geol., Monogr 3.
- Roedder E (1979) Fluid inclusions as samples of ore fluids. In: *Geochemistry of hydrothermal ore deposits*, 2nd ed., Barnes H.L., pp. 684-737, Wiley, New York.
- Roedder E (1984) Fluid inclusions. In: *Reviews in Mineralogy*, Vol. 12, Ribbe P.H., Mineralogical Society of America, 0-939950-16-2, Chelsea-Michigan.
- Ronchi L.H., Touray J.C., Michard A. & Dardenne M.A. (1993). The Riberia fluorite district, Southern Brazil. Geological and geochemical (REE, Sm-Nd isotopes) characteristics. *Mineralium Deposita*, 28, pp. 40-252.
- Rose A.W., Hawkes H.E. & Webb J.S. (1979). *Geochemistry in mineral exploration*. Academic Press, ISBN 0-12-596252-5, London.
- Rouvier H., Perthuisot V. & Mansouri A. (1985). Deposits and salt bearing diapirs in Southern Europe and North Africa. *Economic Geology*, 80, pp. 666-687.

- Ruiz J., Richardson C.K. & Patchett P.J. (1988). Strontium isotope geochemistry of fluorite, calcite, and barite of the Cave-in-rock Fluorite District, Illinois. *Economic Geology*, 83, pp. 203-210.
- Sainfeld P. (1952). *Les gîtes plombo-zincifères de la Tunisie*. Annales des Mines et de la Géologie, n° 9, Société Française d'Éditions en Afrique du Nord, Tunis.
- Sallet R., Moritz R. & Fontignie D. (2000). Fluorite $^{87}\text{Sr}/^{86}\text{Sr}$ and REE constraints on fluid-melt relations, crystallization time span and bulk D^{Sr} of evolved high-silica granites. Tabuleiro granites, Santa Catarina, Brazil. *Chemical Geology*, 164, pp. 81-92.
- Sallet R., Moritz R. & Fontignie D. (2005). The use of vein fluorite as probe for paleofluid REE and Sr-Nd isotope geochemistry: The Santa Catarina Fluorite District, Southern Brazil. *Chemical Geology*, 223, pp. (27-248).
- Sangster D.F., Nowlan G.S. & McCracken A.D. (1994). Thermal comparison of Mississippi Valley-type lead-zinc deposits and their host rocks using fluid inclusion and Conodont colour alteration index data. *Economic Geology*, 59, pp. 493-544.
- Sassi A. (1999). Les phosphates dans les bassins paléogènes de la partie méridionale de l'Axe Nord-Sud (Tunisie). *Thèse doctorat ès Sciences*, Université de Tunis El Manar.
- Savard M.M., Chi G., Sami T., Williams-Jones A.E. & Leigh K. (2000). Fluid inclusion and carbon, oxygen and strontium isotope study of the Polaris Mississippi Valley-type Zn-Pb deposit, Canadian Arctic Archipelago: implications for ore genesis. *Mineralium Deposita*, 35, pp. 495-510.
- Sawkins F.J. (1968). The significance of Na/K and Cl/SO₄ ratios in fluid inclusions and surface waters, with respect to the genesis of Mississippi Valley-type deposits. *Econ Geol*, 63, pp. 935-942.
- Schneider H.J., Möller P. & Parekh P.P. (1975). Rare earth elements distribution in fluorites and carbonate sediments of the East-Alpine Mid-Triassic sequences in the Nordliche Kalkalpen. *Mineralium Deposita*, 10, pp. 330-344.
- Schneider H.J., Möller P., Parekh P.P. & Zimmer E. (1977). Fluorine contents in carbonate sequences and rare earths distribution in fluorites of Pb-Zn deposits in East-Alpine Mid-Triassic. *Mineralium Deposita*, 12, pp. 22-36.
- Schönenberger J., Köhler J. & Markl G. (2008). REE systematics of fluorides, calcite and siderite in peralkaline plutonic rocks from the Gradar Province, South Greenland. *Chemical Geology*, 247, pp. 16-35.
- Schwinn G. & Markl G. (2005). REE systematics in hydrothermal fluorite. *Chemical Geology*, 216, pp. 225-248.
- Shepherd T.J., Darbyshire D.P.F., Moore G.R. & Greenwood D.A. (1982). Rare earth element and isotopic geochemistry of the North Pennine ore deposits. *Bulletin du BRGM*, section II (4), pp. 371-377.
- Shepherd T.J., Rankin A.H., Alderton D.H.M. (1985). A practical guide to fluid inclusion studies. Blackie and Sons, pp. 229. ISBN 0-216-91646-1, Glasgow.
- Sheppard, S.M.F., Charef, A. & Bouhlef S. (1996). Diapirs and Zn-Pb mineralization: a general model based on Tunisian (N. Africa) and Gulf Coast (U.S.A) deposits. In: Carbonate-hosted lead-zinc deposits, Sangster D.F., pp. 230-243, Society of Economic Geologists Special Publication 4, ISBN 1-887483-95-0, Michigan.
- Souissi F. (1987). Etude gîtologique et conditions de formation des gisements de fluorine (Pb-Zn-Ba) du Jebel Zaghouan (J. Stah et Sidi Taya) et du Jebel Oust, Tunisie nord-orientale. *PhD thesis*, University of Toulouse III.

- Souissi F., Fortuné J.P., Sassi R. & Bouhleb S. (1996). L'association fluorine-cuivre gris du J. Oust (Tunisie nord-orientale). Géologie, minéralogie et inclusions fluides. *Notes du Service Géologique de Tunisie*, 62, pp. 89-104.
- Souissi F., Dandurand J.L. & Fortuné J.P. (1997). Thermal and chemical evolution of fluids during fluorite deposition in the Zaghouan province (north-eastern Tunisia). *Mineralium Deposita*, 32, pp. 257-270.
- Souissi F., Fortuné J.P. & Sassi R. (1998). La minéralisation fluorée de type Mississippi Valley du Jebel Stah (Tunisie nord-orientale). *Bulletin de la Société Géologique de France*, 169 (2), pp. 163-175.
- Souissi F., Sassi R., Bouhleb S., Dandurand J.L. & Ben Hamda S. (2007). Fluid inclusion microthermometry and rare earth element distribution in the celestite of the Jebel Doghra ore deposit (Dome zone, Northern Tunisia): towards a new genetic model. *Bulletin de la Société Géologique de France*, 178, pp. 459-471.
- Souissi F., Souissi R. & Dandurand J. (2010). The Mississippi Valley-type fluorite ore at Jebel Stah (Zaghouan district, north-eastern Tunisia): contribution of REE and Sr isotope geochemistries to the genetic model. *Ore Geology Reviews*, 37, pp. 15-30.
- Spangenberg J., Sharp Z.D & Fontboté L. (1993). Apparent stable isotope heterogeneities in carbonates due to the effect of organic matter and sulphides: Case study on the San Vicente MVT zinc-lead deposit, Peru. In: *Current Research in Geology Applied to Ore Deposits*, Fenoll Hach-Ali P., Torres-Ruiz F. & Gervilla F., pp. 241-244, Proceedings of the second biennial SGA Meeting, 84-338-1772-8, Granada.
- Spangenberg J., Sharp Z.D & Fontboté L. (1995). Apparent stable isotope heterogeneities in gangue carbonates of the Mississippi Valley-type Zn-Pb deposit of San Vicente, Central Peru. *Mineralium Deposita*, 30, pp. 67-74.
- Strong D.F., Fryer B.J. & Kerrich R. (1984). Genesis of the St Lawrence fluorite deposit as indicated by fluid inclusion, rare earth element, and isotopic data. *Economic Geology*, 79, pp. 1142-1158.
- Strubel G. (1965). Quantitative Untersuchungen über die hydrothermale Löslichkeit von Fluospat (CaF_2). *Neues Jahrb Min*, 3, pp. 83-95.
- Subias I. & Fernandez-Nieto C. (1993). REE fractionation and fluid inclusion studies in fluorites from the Valle de Tena (Spanish Central Pyrenees). In: *Current Research in Geology Applied to Ore Deposits*, Fenoll Hach-Ali P., Torres-Ruiz F. & Gervilla F., pp. (249-252), Proceedings of the 2nd biennial SGA Meeting, ISBN 84-338-1772-8, Granada.
- Sverjensky D.A. (1984). Europium redox equilibria in aqueous solution. *Earth and Planetary Science Letters*, 67, pp. 70-78.
- Taylor S.R. & McLennan S.M. (1985). *The continental crust: its composition and evolution. An examination of the geochemical record preserved in sedimentary rocks*. Blackwell, ISBN 0-632-01148-3, Oxford.
- Thibieroz J. (1974). Hammam Jedidi et Hammam Zriba: étude géologique et minière de deux gisements stratiformes dans le cadre de la province fluorée tunisienne; l'association des concentrations fluorée aux surfaces d'émergence. *Thèse 3ème cycle*, Université de Paris VI.
- Thibieroz J. (1976). Reconstitution chronologique du rôle des surface d'émergence dans l'histoire du gisement de fluorite de Hammam Zriba (région de Zaghouan-Tunisie). *Mém. H. s. Soc. géol. Fr.*, 7, pp. 33-37.

- Thibieroz J. (1982). Typologie des gîtes de fluorine. Répartition des gisements en France et dans les régions voisines. *Bulletin du BRGM*, section II (4), pp. 437-449.
- Touhami A. (1979). Contribution à l'étude géologique et métallogénique de la province fluorée tunisienne; rôle de l'altération superficielle dans la formation des concentrations fluorées. *Thèse 3ème Cycle*, Université de Tunis.
- Trona F. (1973). Position des horizons dolomitiques minéralisés en fluorine et galène au sein des sédiments triasiques de la Sierra de Lujar (Grenade. Evolution et géochimie. *Thèse Doctorat ès Sciences*, Paris.
- Tropper P. & Manning C.E. (2007). The solubility of fluorite in H₂O and H₂O-NaCl at high pressure and temperature. *Chemical Geology*, 242, pp. 299-306.
- Turki M.M. (1988). Polycinématique et contrôle sédimentaire associé sur la cicatrice Zaghouan-Nebhana. *Thèse Doctorat ès Sciences*, Université de Tunis.
- Uysal I.T., Zhao J.X., Golding S.D., Lawrence M.G., Glikson M. & Collerson K.D. (2008). Sm-Nd dating and rare-earth element tracing of calcite: Implications for fluid-flow events in the Bowen Basin, Australia. *Chemical Geology*, 238, pp. 63-71.
- Valenza K., Moritz R., Mouttaqi A., Fontignie D. & Sharp Z. (2000). Vein and Karst Barite Deposits in the Western Jebilet of Morocco: Fluid Inclusion and Isotope (S, O, Sr) Evidence for Regional Fluid Mixing Related to Central Atlantic Rifting. *Economic Geology*, 95, pp. 587-606.
- Vietz J.C. & Leach D.L. (1990). Genetic implications of regional and temporal trends in ore fluid geochemistry of Mississippi Valley-type deposits in the Ozark region. *Economic Geology*, 85, pp. 842-861.
- Weisbrod A. & Poty B. (1975). Thermodynamics and geochemistry of the hydrothermal evolution of the Mayres pegmatite, Southeastern Massif Central (France). *Pétrologie*, Part 11, pp. 1-16.
- Zimmerman R.K. & Kesler S.E. (1981). Fluid inclusions evidence for solution mixing. Sweetwater (Mississippi Valley) district, Tennessee. *Economic Geology*, 76, pp. 134-142.

IntechOpen



Geochemistry - Earth's System Processes

Edited by Dr. Dionisios Panagiotaras

ISBN 978-953-51-0586-2

Hard cover, 500 pages

Publisher InTech

Published online 02, May, 2012

Published in print edition May, 2012

This book brings together the knowledge from a variety of topics within the field of geochemistry. The audience for this book consists of a multitude of scientists such as physicists, geologists, technologists, petroleum engineers, volcanologists, geochemists and government agencies. The topics represented facilitate as establishing a starting point for new ideas and further contributions. An effective management of geological and environmental issues requires the understanding of recent research in minerals, soil, ores, rocks, water, sediments. The use of geostatistical and geochemical methods relies heavily on the extraction of this book. The research presented was carried out by experts and is therefore highly recommended to scientists, under- and post-graduate students who want to gain knowledge about the recent developments in geochemistry and benefit from an enhanced understanding of the dynamics of the earth's system processes.

How to reference

In order to correctly reference this scholarly work, feel free to copy and paste the following:

Fouad Souissi, Radhia Souissi and Jean-Louis Dandurand (2012). The Genesis of the Mississippi Valley-Type Fluorite Ore at Jebel Stah (Zaghouan District, North-Eastern Tunisia) Constrained by Thermal and Chemical Properties of Fluids and REE and Sr Isotope Geochemistry, *Geochemistry - Earth's System Processes*, Dr. Dionisios Panagiotaras (Ed.), ISBN: 978-953-51-0586-2, InTech, Available from: <http://www.intechopen.com/books/geochemistry-earth-s-system-processes/genesis-of-the-mississippi-valley-type-fluorite-ore-at-jebel-stah-zaghouan-district-north-eastern-tu>

INTECH
open science | open minds

InTech Europe

University Campus STeP Ri
Slavka Krautzeka 83/A
51000 Rijeka, Croatia
Phone: +385 (51) 770 447
Fax: +385 (51) 686 166
www.intechopen.com

InTech China

Unit 405, Office Block, Hotel Equatorial Shanghai
No.65, Yan An Road (West), Shanghai, 200040, China
中国上海市延安西路65号上海国际贵都大饭店办公楼405单元
Phone: +86-21-62489820
Fax: +86-21-62489821

© 2012 The Author(s). Licensee IntechOpen. This is an open access article distributed under the terms of the [Creative Commons Attribution 3.0 License](#), which permits unrestricted use, distribution, and reproduction in any medium, provided the original work is properly cited.

IntechOpen

IntechOpen